Progress in Nuclear Energy 104 (2018) 342–358

Contents lists available at ScienceDirect

Progress in Nuclear Energy

journal homepage: www.elsevier.com/locate/pnucene

Review of recent experimental results on the behavior of actinide-bearing oxides and related materials in extreme environments

Cameron L. Tracy [a], Maik Lang [b], Fuxiang Zhang [c], Sulgiye Park [a], Raul I. Palomares [b], Rodney C. Ewing [a, *]

[a] Department of Geological Sciences, Stanford University, Stanford, CA 94305, USA
[b] Department of Nuclear Engineering, University of Tennessee, Knoxville, TN 37996, USA
[c] Materials Science and Technology Division, Oak Ridge National Laboratory, Oak Ridge, TN 37831, USA

ARTICLE INFO

Article history:
Received 18 December 2014
Received in revised form
18 July 2016
Accepted 11 September 2016
Available online 16 September 2016

Keywords:
Nuclear materials
Radiation effects
High temperature
High pressure
Phase transformations
Nuclear fuels
Complex oxides

ABSTRACT

Oxide materials find use throughout the nuclear fuel cycle, from actinide-bearing ores and commercial reactor fuels to wasteforms for radionuclide disposal. In geological, reactor, and waste repository conditions, these materials are often exposed to ionizing radiation, high temperatures, and mechanical stresses. Recently, a large body of work has investigated the response of actinide oxides and analogue compounds to extreme environments, including the individual and combined effects of radiation, temperature, and pressure. Study of the phase behavior of these materials under such conditions can lead to improved understanding of their stability throughout the nuclear fuel cycle, as well as strategies for the mitigation of associated performance degradation. This article reviews some recent experimental work on this topic, highlighting advanced techniques developed for the exposure of materials to extreme environments, and for the *in situ* characterization of their structural and chemical responses. The study of two classes of nuclear materials is reviewed: binary oxides typical of nuclear fuels, and complex oxides typical of geological materials and wasteforms. Particular emphasis is placed on the individual and combined effects of modifications to the atomic and electronic structures of materials by exposure to extreme environments.

1. Introduction

Oxides are found throughout the nuclear fuel cycle, most often as actinide-bearing materials. Uranium is extracted from ores consisting primarily of the mineral uraninite (UO_{2+x}), along with coffinite ($USiO_4$) and brannerite (UTi_2O_6) (Finch and Murakami, 1999). Solid mill tailings, usually disposed of near uranium ore mines, are composed of various actinide-bearing silicate, sulfate, and oxyhydroxide minerals (Abdelouas, 2006). Most commercial nuclear reactors use UO_2 as a fissile fuel, sometimes accompanied by PuO_2 in mixed oxide (MOX) fuels. Many proposed methods for actinide waste management, including geological disposal and transmutation to shorter-lived isotopes in inert matrix fuels (IMFs), require the development of stable materials to dilute and immobilize radionuclides (Degueldre and Paratte, 1999; Degueldre, 2007; Ewing, 2011). Complex oxides, based on minerals that are known to incorporate actinides over geological timescales, have garnered substantial interest for this purpose (Ewing, 2011, 2007; Ewing et al., 2004; Lumpkin, 2001). Finally, the interaction of nuclear fuel with groundwater or coolant, as can occur in a reactor accident or cladding failure scenario, can yield various oxyhydroxide, carbonate, silicate, and phosphate phases (Burns et al., 2012).

Common to all such actinide-bearing oxide nuclear materials is their exposure to extreme environments including energetic radiation, high temperatures, and high pressures or stresses. Ionizing radiation, wherein particles of high specific energy (above approximately 1 MeV/u) interact with matter primarily via electronic excitation, is particularly relevant for actinide-bearing nuclear materials (Matzke, 1992). It is encountered in the form of alpha particles produced by radionuclide decay (helium nuclei with typical energies around 5 MeV) and fission fragments produced by

* Corresponding author.
E-mail address: rewing1@stanford.edu (R.C. Ewing).

http://dx.doi.org/10.1016/j.pnucene.2016.09.012
0149-1970/

the induced or spontaneous fission of actinides (heavy element nuclei with energies of 80–120 MeV). Atomic displacement can result from either the modification of interatomic forces following excitation of electrons from bonding to antibonding orbitals, or local heating due to phonon emission during the non-radiative decay of excited electrons (Duffy et al., 2012). These displacements can generate diverse defects and phase modifications in the irradiated material (Zhang et al., 2011a,b). In the case of fission fragments, ionizing radiation produces cylindrical "ion tracks" of damage with diameters around 10 nm and lengths of up to tens of micrometers. The nanoscale, highly transient thermal spike that accompanies particle-solid interactions at high specific energies produces very high local temperatures and pressures (Ronchi and Wiss, 2002), along with atomic displacement and modified interatomic forces (Duffy et al., 2012), making the interior of an ion track an extreme environment. Exposure of nuclear materials to highly ionizing radiation can cause degradation of properties important to their performance, such as thermal conductivity (West et al., 1968).

Nuclear fission and decay also induce bulk heating of radionuclide-bearing materials, requiring them to operate under high temperatures that can alter phase stability and modify the kinetics of atomistic processes. High pressures are encountered in reactors in the form of stresses caused by, for example, fuel swelling or cladding failure. Such loading is generally localized. Stresses at crack tips, for example, can be much higher than those applied to bulk fuel pellets. High pressure is also encountered in geological conditions which, while not directly related to nuclear fuel performance, are relevant to the mineralogy of actinide-bearing ores from which fuel materials are extracted. Within Earth's mantle, where pressures on the order of 10 GPa are encountered, there exist significant quantities of natural uranium and thorium (Helffrich and Wood, 2001; Turcotte et al., 2001). The phases in which this material is incorporated are not known, so study of the behavior of actinide oxides at high temperature and high pressure is needed to constrain their geological behavior. As with temperature, changes in pressure can significantly modify the phase stability of a material.

These extreme conditions limit the performance and operational lifetime of actinide oxide components throughout the nuclear fuel cycle. Understanding the responses of actinide-bearing materials to extreme environments is necessary to improve the efficiency and safety of nuclear energy generation. For example, achieving increased burn-ups in nuclear fuels is economically favorable, but requires mitigation of the fuel performance degradation induced by in-reactor radiation and high temperatures (Grimes et al., 2008). The development of suitable wasteforms for actinides requires the development of materials that are structurally and chemically stable under crustal conditions for the long periods of time during which these wastes remain dangerously radioactive (Ewing, 2011, 2007). Tolerance of extreme environments is also important with respect to the development of Gen IV reactors, which are planned to operate under conditions more extreme than those of current Gen III facilities (Grimes et al., 2008). For these reasons, significant effort has been dedicated, in recent years, to study of the behavior of actinide oxide materials in extreme environments. Recently, emphasis has been placed on the use of combined extreme conditions of irradiation, temperature, and pressure. This allows for more accurate simulation of the conditions encountered in the operating environments of nuclear materials. For example, irradiation of a material under high temperature or pressure can modify the character of the damage induced, compared with irradiation at ambient conditions, and the radiation tolerance of a nuclear component is therefore dependent on these parameters. Additionally, experimental study of material behavior at far-from-equilibrium conditions, beyond those that might be encountered in the nuclear fuel cycle, provides insight into the fundamental mechanisms controlling the phase responses of actinide materials to irradiation, heating, and the application of mechanical stresses. Better understanding of these behaviors at the atomistic scale is crucial to modeling and simulation efforts.

Experimental study of the behavior of nuclear materials in extreme environments is necessarily restricted by the safety precautions required for such work. To minimize the risk of radionuclide release and the associated regulatory burden, studies of actinide materials are often limited to small sample volumes, making many techniques that require the use of large bulk samples unsuitable for this purpose. Additionally, containment of the samples is usually necessary, which can render samples inaccessible to certain experimental probes. However, advanced experimental techniques, many based on the use of synchrotron radiation (Shi et al., 2014), have been developed to allow for observation of the structural effects of irradiation, temperature, and pressure on actinide materials. Additionally, some insight into the potential behavior of actinide-bearing materials can be gained from the study of lanthanide-bearing materials, given their similarities in crystal chemistry and thermophysical properties. This manuscript reviews recent developments in the experimental study of the response of actinide-bearing oxide nuclear materials, and some non-actinide analogue materials, to extreme environments. Emphasis is placed on the responses of these compounds to ionizing radiation, high temperature, and high pressure. While property degradation is of primary interest from a nuclear engineering outlook, this review focuses instead on the underlying structural and crystal chemical responses of nuclear materials to these conditions, which yield mechanistic insight into the processes controlling the tolerance of nuclear materials for extreme conditions.

This review focuses on experiments that seek to access extremes of temperature (on the order of 1000 K), pressure (on the order of 10 GPa), and energy deposition by radiation (particle energies in the MeV-GeV range and resulting target energy densities on the order of 10 eV/atom). These are not necessarily representative of the conditions most frequently encountered in the nuclear fuel cycle, and instead represent the conditions most challenging to simulate in laboratory experiments. For example, pressures in the GPa range are not typically encountered by nuclear fuels, and the applications of studies under these conditions pertain mainly to the behavior of materials in Earth's mantle. However, such basic science can be of great importance for materials design throughout the nuclear fuel cycle. For example, high pressure equations of state for actinide materials have been used to quantify the damage induced in UO_2 by fission fragment irradiation (Ronchi and Wiss, 2002). This demonstrates the connection between studies of nuclear material behavior in a pressure regime far beyond that which might be encountered under reactor conditions, and the in-reactor behavior of a nuclear fuel.

The radiation energy range addressed in this review largely limits its scope to radiation-induced electronic excitation, excluding study of the elastic collisions between nuclei that dominate energy transfer in the case of neutron and alpha decay recoil damage. Readers are referred to earlier reviews which comprehensively discuss radiation damage in this and other energy regimes (Hobbs et al., 1994; Robinson, 1994; Weber and Ewing, 1998). Additionally, it is important to consider separately the steady state behavior of materials in extreme environments and the responses of materials to transient application of temperature and pressure. Due to the limited data available regarding the behavior of actinide-bearing materials in these transient conditions, results obtained using relatively slow heating, cooling, and pressurization rates are emphasized here. For the purposes of this review,

actinide-bearing oxide nuclear materials are delineated into two categories: simple binary oxides, which are characteristic of nuclear fuels, and complex oxides, which are characteristic of synthetic wasteforms and natural actinide bearing minerals.

2. Experimental techniques

2.1. Extreme environments

Irradiation with ions of high specific energy, to simulate the effects of either alpha particles or fission fragments, can be accomplished through self-irradiation of a radioactive material, exposure to a radioactive source, or exposure to an ion beam generated by a particle accelerator. Alpha particle self-irradiation of a material can be performed for materials in which an alpha-emitter is a major component, or which has been doped with an alpha emitter (Sykora et al., 2005; Wiss et al., 2014) (note that references given in this section are not comprehensive, and instead provide representative examples of the use of a particular technique). This approach can produce highly homogeneous alpha particle exposure. However, alpha particle emission also entails the recoil of the nucleus from which the particle is emitted. Alpha recoils introduce damage to the sample material through elastic nuclear collisions with adjacent atoms. The local thermal spikes produced from these recoil events can reduce the total damage produced by a single alpha emission event due to annealing effects. Such alpha annealing has been demonstrated for PuO_2 and UO_2 (Weber, 1984, 1981). This behavior makes it difficult to isolate the effects of energy deposition by ionization from those of elastic nuclear collisions, and vice versa. Alternatively, an alpha source, such as $^{238}PuO_2$, can be placed in close proximity to the sample (Weber, 1981). However, the limited penetration depth of alpha particles in solids means that this technique yields only thin irradiated layers in the sample material and is prone to surface effects. The use of an ion accelerator gives well-aligned particle paths, enabling study of radiation damage as a function of penetration depth (Guimbretière et al., 2012). Additionally, such a technique allows for the use of high particle flux, reducing the time necessary to reach the desired alpha particle dose, as compared with self-irradiation. Still, the flux must be limited to avoid bulk heating of samples. Because alpha particles have relatively low energies, in comparison to fission fragments, the necessary accelerators are typically laboratory-scale. If the goal of an experiment is to simulate a specific nuclear material operating environment (*e.g.*, geological disposal or reactor conditions), care must be taken to select a radiation source that is suitable with respect to particle energy, mass, flux, and the presence of emission recoil nuclei.

Fission fragment irradiations are typically more difficult than alpha particle irradiations, from an experimental standpoint. Spontaneous fission rates are generally low, such that self-irradiated samples must be either of natural origin and of an age suitable for significant fission fragment damage to have accumulated (Fleischer, 2004), or be irradiated in a nuclear reactor to induce fission (Mieszczynski et al., 2014, 2012; Nogita and Une, 1994). The former method limits the materials that can be studied to the minerals that incorporate actinides in sufficient concentration, while the latter results in highly radioactive samples that often necessitate hot labs or other dedicated facilities for examination. In-reactor irradiation also introduces damage from elastic collisions of neutrons with nuclei in the sample material, the effects of which can be difficult to distinguish from those of fission fragments. Additionally, self-irradiation unavoidably leads to the inclusion of various soluble and non-soluble fission products in the irradiated material, the structural effects of which can be difficult to deconvolute from those of radiation-induced defects (Mieszczynski et al., 2014). However, these techniques can be advantageous in that they precisely mimic the operating conditions of commercial nuclear materials. Many studies instead make use of large accelerator facilities capable of producing beams of high energy, heavy ions, known as “swift heavy ions”. Such facilities include the GSI Helmholtz Centre for Heavy Ion Research in Darmstadt, Germany, the Joint Institute for Nuclear Research in Dubna, Russia, the JAEA tandem accelerator in Tōkai, Japan, and the Heavy Ion Research Facility in Lanzhou, China, among others. As with lower energy ion beam irradiations, the beam flux must be considered if heating of the sample is not desired. Swift heavy ions typically have ranges in solids on the order of 10–100 μm, so thin specimens can be prepared if complete penetration of the sample is desired. In this approach, all ions traverse irradiated samples, parallel to one another, and exit the opposite side of the sample with no implantation occurring. This can aid in determination of the damage resulting from isolated ion tracks, and in quantitative analysis of the effects of track overlap. However, compared to self-irradiation, these experimental conditions are less representative of those encountered by actinide materials in the nuclear fuel cycle. Analysis of materials with randomly oriented fission fragment tracks is particularly important when crystallite orientation effects are considered (Mieszczynski et al., 2014).

The temperature of oxide materials can be controlled through the use of either resistive heating (Chollet et al., 2013; Lebreton et al., 2012; Vauchy et al., 2014) or laser heating (Böhler et al., 2014a, 2014b; Cappia et al., 2014; Manara et al., 2005a, 2004). The former method generally entails the use of a heated sample stage or holder, which is often coupled to a particular experimental probe for *in situ* measurements. For example, heating stages for x-ray diffractometers and transmission electron microscopes are commonly used to study high temperature phase transformations and defect annealing. This technique allows for precise temperature control through the use of thermocouple monitoring, but requires that the sample be accessible to heating elements or in contact with a sample holder of sufficiently high thermal conductivity for the desired temperature ramp rate. Laser heating, in contrast, requires only that part of the sample container is transparent to the laser. Therefore, it is often advantageous for the study of actinide materials or pressurized materials, as both generally require that samples be sealed, limiting access by heating elements and thermocouples. When using this technique, temperatures can be monitored through use of a pyrometer. However, thermal gradients can be unacceptably high with this form of spot heating.

Pressures on the order of 10 GPa are routinely applied to materials using diamond anvil cells (DACs) (Jayaraman, 1986). In these devices, samples are placed within a metal gasket, along with pressure calibrant materials and a pressure-transmitting medium such as a methanol/ethanol mixture or an inert gas. The gasket is then squeezed between parallel faces of two high hardness diamonds. Because diamond is transparent to x-rays and visible light, diffraction and spectroscopy characterization of samples can be performed *in situ* at high pressure. However, absorption by the diamonds and sample, along with the small volume of the pressure cell, necessitate the use of synchrotron radiation in transmission geometry for diffraction measurements. Pressures within the cell are monitored by measuring, for example, the lattice parameter of gold or the fluorescence wavelength of ruby, both of which are highly sensitive to pressure. The DAC acts as an effective container for loaded samples, which is advantageous for the study of actinide materials. After analysis, the cell can be depressurized and the sample removed for post-pressurization analysis (Zhang et al., 2014b).

These techniques can be applied in sequence or simultaneously. Irradiation can be performed at elevated temperatures by placing

samples containing alpha emitters in a furnace, or by mounting samples on a heating stage exposed to an accelerated ion beam (Sonoda et al., 2006; Wiss, 1999). Recently, methods for the irradiation of samples at high pressure have been developed (Lang et al., 2009c, 2015) wherein DACs are exposed to an ion beam of sufficient energy to penetrate the first diamond and the sample. The low density of diamond results in a low ion stopping power, such that ions of very high energy (swift heavy ions) can be injected into a DAC's sample chamber. Calibration of the ion energy is necessary to ensure that, after traversing the diamond, the ions possess the energy desired for the simulation of fission fragments (Lang et al., 2005). Finally, high pressure and high temperature conditions can be combined via either the laser heating of material inside of a DAC (Boehler and Chopelas, 1991), taking advantage of the visible light transparency of its diamond "windows," or the use of a hydrothermal diamond anvil cell (HDAC), in which heating coils are placed adjacent to the diamonds (Bassett et al., 1993). Because energetic ions can be injected into the diamond anvil cell pressure chamber, these methods allow for the combination of all three extreme conditions (radiation, temperature, and pressure), on a sample which is safely contained in a sealed environment. One potential method for the simultaneous exposure of a sample to extreme conditions of pressure, temperature, and irradiation, as well as an x-ray beam for sample characterization, is illustrated schematically in Fig. 1.

2.2. Materials characterization

Extreme environments induce modifications to oxide nuclear materials across a range of length scales. Both the atomic and electronic structures of such materials can be affected. Therefore, systematic study of these modifications requires the use of numerous complementary characterization techniques. Synchrotron techniques are useful for this purpose, as their intense, high-energy x-ray beams can overcome some of the limitations imposed by the sample environments required for the *in situ* exposure of radioactive materials to extreme conditions (Shi et al., 2014). For example, the highly focused x-ray beams produced by these facilities can often deliver satisfactory signal despite the presence of a sealed sample container. X-ray diffraction (XRD) can be used to monitor the long-range structure of a material. In this way, phase transformations induced by extreme conditions can be tracked as a function of radiation fluence, temperature, or pressure. In conjunction with Rietveld refinement (Rietveld, 1969) of the collected diffraction patterns, changes in lattice parameter can be measured to track radiation-induced defect accumulation, thermal expansion, or compression of a material. Refinement of site occupancies and displacement parameters provides information about structural damage resulting from the displacement of atoms from their ideal sites during irradiation. Analysis of diffraction peak widths via Williamson-Hall methods (Williamson and Hall, 1953) yields quantitative information regarding grain sizes and the presence of heterogeneous microstrain within a sample. Small-angle x-ray scattering (SAXS) can be used to investigate features at larger length scales. In particular, the dimensions and morphologies of fission fragment-induced ion tracks can be measured using this method, which is sensitive to spatial variation in the electron density of a material (Eyal and Abu Saleh, 2007). Finally, modification of a material's crystal chemistry, including oxidation state and coordination changes, can be monitored using x-ray absorption spectroscopy (XAS) (Nishi et al., 2010; Prieur et al., 2014; Tracy et al., 2014, 2015a). This technique is particularly useful for actinide materials, as their 5*f* electrons give rise to complex chemical behavior, which can vary greatly across the actinide series (Conradson et al., 2004a, 2004b). Experimental difficulties arise from the use of XAS with DACs due to diffraction by the single crystal diamond anvils at specific energies, necessitating either rotation of the cell with respect to the x-ray beam (to change the diffraction condition) and collection of multiple absorption spectra (Sapelkin and Bayliss, 2001), or the use of nanocrystalline diamond anvils (Baldini et al., 2011).

Applicable non-synchrotron techniques include Raman spectroscopy, transmission electron microscopy (TEM), and Rutherford backscattering spectrometry in channeling mode (RBS/C). Raman spectroscopy results are often complementary to XRD, as they provide information regarding the short-range structure of materials. Radiation induced defects, in particular, often strongly modify the Raman spectra of a material by inducing a breakdown in the selection rules (Guimbretière et al., 2012; Tracy et al., 2014). RBS/C has been used to measure the radiation-induced structural disorder resulting from atomic displacements and its evolution with increasing dose (Garrido et al., 2009, 1997; Thomé et al., 2013). Unique features of this technique include the ability to obtain depth-dependent data on structural damage and, in some cases, to distinguish damage on the anion and cations sublattices (Garrido et al., 1997). However, these measurements are precluded in instances where sample containment blocks either the incoming ion beam or the backscattered particles. Thus, it is of limited utility for the study of high pressure behavior, as the diamonds and gasket in a DAC will block these particles. TEM enables the direct observation of atomic structure and microstructure modifications to a material. It is frequently used to study ion track phase morphology through cross-sectional imaging of individual tracks (Lang et al., 2009a; Takaki et al., 2014; Zhang et al., 2011b). TEM techniques have also been used to monitor grain size reduction caused by pressurization and subsequent quenching of actinide oxides to ambient conditions (Zhang et al., 2014b). However, *in situ* imaging of material within a DAC is not possible using TEM, so samples must be brought to ambient conditions and removed from the cell before they can be studied in this manner.

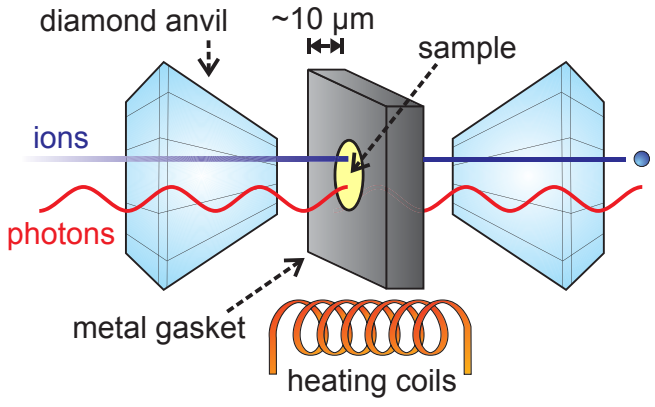

Fig. 1. Schematic illustration of the exposure of a sample to high temperature, high pressure, and irradiation. The sample is held in a thin metal gasket, along with a pressure transmitting medium to ensure quasi-hydrostatic conditions. Diamonds press against both sides of this sample chamber, sealing it in the DAC and applying pressure. Resistive heating coils within the DAC supply heat, and ions from an accelerator are injected through the diamonds and the sample. Photons can also pass through the cell, as in the case of x-ray diffraction or x-ray absorption characterization in transmission mode.

3. Results for binary oxides

All actinides exhibit the fluorite structure (*Fm*-3*m*) as dioxides, AnO_2. This is the stoichiometry of the actinide oxides that is most relevant to nuclear fuels: ThO_2, UO_2, and PuO_2. UO_2 is currently

used in most operating commercial reactors. Powder of PuO_2 is mixed with UO_2 to produce MOX fuel, allowing for partial reprocessing of spent nuclear fuel. ThO_2 is a proposed fuel that allows for in-reactor breeding of fissile uranium in advanced, proliferation-resistant reactor concepts (Lombardi et al., 2008; Lung and Gremm, 2000). Many of the actinide elements also adopt trivalent oxidation states. Plutonium, americium, and curium, all of which are produced by transmutation of uranium during reactor operation, can form sesquioxides, An_2O_3. In contrast, neptunium, another transmutation product, generally retains a tetravalent state and associated fluorite dioxide phase. However, Np_2O_5 can also form. UO_2 can be easily oxidized and exhibits several mixed valence phases up to UO_3. In nuclear fuels, actinides other than uranium typically form a solid solution within a fluorite phase, which contains defects (*e.g.*, oxygen vacancies and interstitials, or local hypo- and hyperstoichiometry) to maintain charge balance. This diverse solid state chemistry and compositional variation in oxidation state stability introduces complexity to the behavior of actinide simple oxides, both individually and in solid solution. Modifications to bonding and redox reactions may occur during irradiation, high temperature, and high pressure (Tracy et al., 2015a; Zhang et al., 2014b). Therefore the behavior of isostructural, thermophysically-similar actinide oxides (*e.g.*, UO_2 and ThO_2) in extreme conditions may differ dramatically due to the accessibility of different oxidation states. Systematic study of these compounds is therefore useful for assessment of the performance of nuclear fuels, particularly with respect to the management of nuclear waste and high burn-up fuels in which extensive transmutation will occur.

3.1. Ionizing radiation

Materials with the fluorite structure are known to be highly resistant to radiation damage (Garrido et al., 2009; Sickafus et al., 2007, 2000). They are generally able to incorporate radiation-induced point defects into their structures without undergoing a phase transformation. Early observation of this defect accumulation in fuel materials was performed by TEM. Fission fragment tracks were observed in UO_2 and ThO_2 exposed to both radioactive sources and self-irradiation (Chute, 1967; Noggle and Stiegler, 1960; Ronchi, 1973). Point defect clusters produced by alpha particle irradiation were also observed in ThO_2 (Douglass and Bronisz, 1971). Recent work has made use of accelerators to measure the particle energy and particle mass dependence of ion track radii in UO_2 at energies close to those of fission fragments (Ishikawa et al., 2013; Wiss and Matzke, 1997). Interestingly, fission fragment tracks have not been observed in bulk UO_2 fuel irradiated in-reactor (Wiss and Matzke, 1997). This suggests that the reported TEM observation of such tracks in out-of-reactor irradiated materials might be dependent on the use of thin, electron-transparent foils during irradiation. Thus, it is possible that the formation of observable tracks is solely a surface effect. Alternatively, it might be the case that tracks are only observable at low fission fragment doses, and that the overlap of tracks at doses characteristic of spent fuel renders them undetectable. Finally, it is also possible that the high temperatures under which nuclear fuels operate cause annealing of tracks, although tracks have been observed by TEM in isostructural CeO_2 irradiated at temperatures near those of the relatively cool rim region of nuclear fuel pellets (Sonoda et al., 2006). This discrepancy between the results of irradiation using accelerators and in-reactor irradiation is problematic, as it limits the applicability of the former technique to the study of nuclear fuel behavior. Systematic study of the dependence of track visibility on penetration depth, particle flux, and temperature is needed to resolve this issue.

While useful, this conventional TEM observation of ion track-induced contrast has yielded little insight into the atomic-scale modifications induced by ionizing radiation, or on the structures of track interiors. Recently, application of advanced scanning transmission electron microscopy (STEM) techniques to CeO_2 irradiated with ions of fission fragment energies has been reported (Takaki et al., 2014), elucidating the specific effects of such radiation on the in-track structure of a fluorite material. Takaki et al. observed a reduction in the atomic density of a nanometric track core region, indicating the expulsion of matter from this track core into a surrounding track shell. This process yields segregation of the vacancy and interstitial components of radiation-induced Frenkel defects. Notably, this segregation was found to occur preferentially on the anion sublattice, suggesting the production of local fluctuations in stoichiometry within an ion track. XAS measurements of CeO_2 irradiated under similar conditions have demonstrated irradiation-induced oxidation state reduction of Ce^{4+} to Ce^{3+}, a process that would be required to maintain charge neutrality in the presence of local nonstoichiometry (Tracy et al., 2015a). Future application of such techniques to the study of actinide oxides might yield interesting insight into both the atomic structures of ion tracks in nuclear fuels and the potential influence of complex actinide redox chemistry on the response of these materials to ionizing radiation, given this evidence of stoichiometry variation within tracks. In particular, study of UO_2 and ThO_2 using this technique could provide insight into the role of the observed local stoichiometry changes in radiation damage accumulation, as uranium oxides are prone to nonstoichiometry, whereas thorium oxides are not.

Following the observation of fission track damage in nuclear fuels via TEM, study of the effects of this radiation on the long-range structure of these materials was performed by XRD characterization. By collecting diffraction data from UO_2 irradiated in-reactor to various fission doses, a unit cell parameter increase was observed with increasing dose (Nakae et al., 1979, 1978a, 1978b). This effect was attributed to the accumulation of defects and the associated additional volume they occupy, compared to an atom occupying an ideal fluorite structure site. Recently, detailed XRD analysis of UO_2 and MOX fuel (4.7 wt% PuO_2) irradiated in reactors has been performed, yielding quantitative measurements of both unit cell expansion and heterogeneous microstrain (Mieszczynski et al., 2014, 2012). This study shows reasonable agreement with those of Nakae et al., reporting post-irradiation unit cell expansions on the order of 0.1%. This effect has been attributed primarily to irradiation-induced defect formation, with minimal influence of fission product accumulation (Mieszczynski et al., 2014). The use of accelerators has allowed precise tracking of this unit cell parameter change as a function of ion fluence (Hayashi et al., 1997, 1994). In addition to lattice expansion, fission fragment-induced defects have been identified as a possible cause of the formation of the nuclear fuel “rim structure” at high fluence (Nogita and Une, 1994; Sonoda et al., 2010). Thus, study of these defects is important with respect to the mitigation of a key nuclear fuel degradation process.

Similar study on other fuel materials and analogues, such as ThO_2 and CeO_2 (Tracy et al., 2014, 2015a), has allowed for direct comparison of the radiation tolerance of different materials. Fig. 2a,b displays representative data obtained from such experiments, while Fig. 2c compares damage accumulation as a function of fluence, derived from the refinement of XRD patterns, for UO_2 and ThO_2. Damage accumulation in both can be approximated by a single-impact model, wherein damage is assumed to result from the impact of a single ion with a certain volume of material, with no effect of track overlap (Weber, 2000). This gives rise to the initially linear buildup of damage, followed by saturation as the ion tracks begin to overlap. However, the rate of damage accumulation and

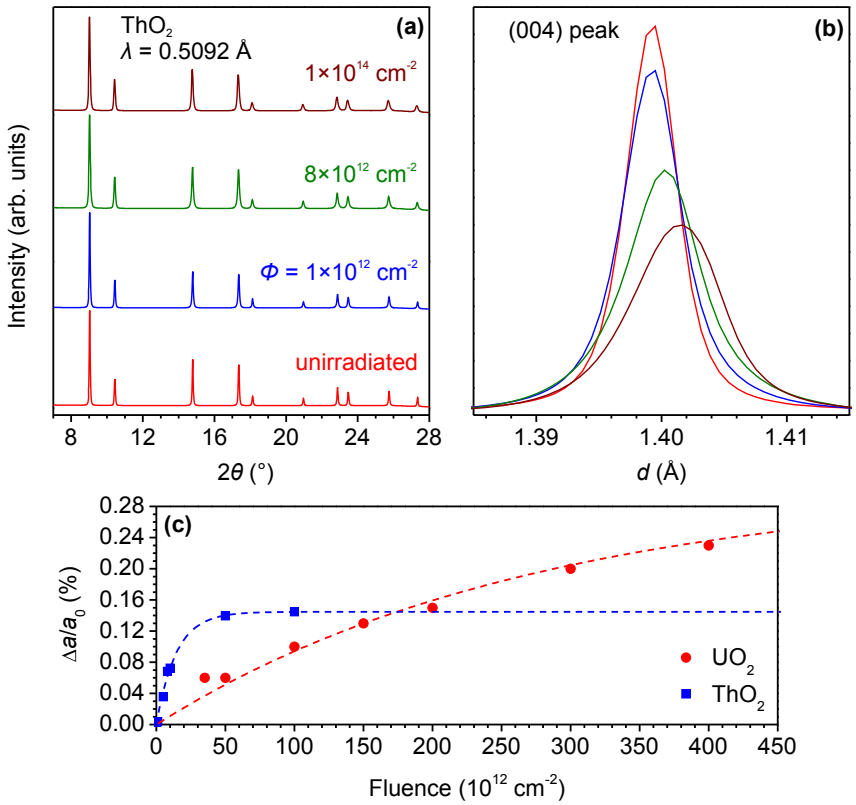

Fig. 2. a) XRD patterns of ThO_2 irradiated with 167 MeV Xe ions, shown for multiple ion fluences. Three modifications are evident in the patterns: attenuation, broadening, and angular shifts of the diffraction maxima. The patterns were measured in transmission mode and the indicated wavelength, λ, refers to the wavelength of the x-rays used in this measurement. **b)** Shifts in the (400) diffraction peak positions in d-space during irradiation. **c)** Lattice parameter values refined as a function of ion fluence for ThO_2 irradiated with 167 MeV Xe ions and UO_2 irradiated with 100 MeV I ions. The UO_2 data was adapted from (Hayashi et al., 1997). Both data sets are fit with a single impact model (Weber, 2000).

the saturation values differ dramatically between the two materials. Such a finding is relevant to the development of advanced fuels with variable compositions, and can also yield insight into the mechanisms of damage accumulation in these materials. Studies on the structural response of UO_2 to low ion fluences and comparison with the response of ThO_2 might further clarify the character of the defects produced by radiation in this high specific energy regime. Study of radiation damage in ThO_2 at fluences above the apparent saturation of damage is also needed, since UO_2 still exhibits significant accumulation of damage at these high fluences.

The exceptionally slow buildup of damage in UO_2 suggests that the former material may not exhibit purely single-impact behavior. Multiple ion impacts may be necessary to induce a unit cell parameter increase within a UO_2 ion track, in contrast to the behavior of ThO_2. However, the lack of data at low fluences, during which damage accumulates rapidly in ThO_2, makes it difficult to assess this behavior. The observed dramatic deviation in the behavior of two isostructural actinide compounds may be related to differences in the stable electronic configurations of these materials. Multiple oxidation states are accessible to uranium in an oxide, whereas states other than Th^{4+} have not been observed in thorium oxides. As such, uranium dioxide can be easily oxidized under extreme conditions, with the loss of its 5*f* electrons, while thorium cannot. The radiation-induced changes in local stoichiometry discussed above may yield different behaviors in these otherwise similar materials. Comparison of the radiation responses of ThO_2 and CeO_2 (for which cerium has an accessible trivalent state) has demonstrated an influence of irradiation-induced redox behavior on the induced unit cell parameter change (Tracy et al., 2014). Fig. 3 illustrates schematically the manner in which ionization-driven changes in the oxidation state of a cation can yield structural distortions similar to those caused by atomic displacement. These results attest to the potential for variation in electronic configuration across the actinide series to influence the responses of actinide oxides to extreme environments.

Comparative investigation of defect-induced unit cell expansion has also been performed on CeO_2, UO_2, and PuO_2 irradiated with alpha particles (Weber, 1984). Interestingly, UO_2 was found to be less tolerant of radiation than PuO_2, with more damage exhibited at a given alpha dose. Comparison of AmO_2 and Am_2O_3 has shown the hexagonal phase of the sesquioxide to be slightly more radiation tolerant than other americium oxide phases (Horlait et al., 2014). As is the case for fission fragment irradiations, experiments focused on the underlying physical processes governing radiation damage are needed to show why these radiation tolerance variations exist. Recent application of spectroscopic techniques to the study of actinide oxide radiation responses has provided intriguing results in this respect. XAS characterization of an alpha irradiated (U,Am)O_2 solid solution indicated partial oxidation of uranium, without a concomitant change in the valence of americium (Prieur et al., 2012). This effect could be related to the ionizing radiation-induced local stoichiometry changes discussed above (Takaki et al., 2014). Uranium is known to easily adopt oxidation states above tetravalent in oxides, while americium has not been observed in a bulk oxide with higher oxidation states. Thus, these results again suggest that changes in the redox chemistry of a material can, to some degree, influence its radiation response. Raman spectroscopy characterization of UO_2 irradiated with simulated alpha particles has provided further evidence of local stoichiometry variation (Guimbretière et al., 2012). Following

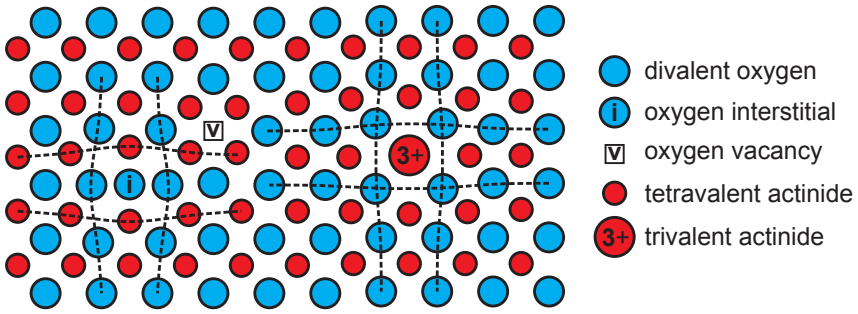

Fig. 3. Illustration of two modes of structural distortion in an irradiated actinide dioxide. On the left side, an anion has been displaced to an interstitial site, producing an anti-Frenkel pair. Local distortion is produced around each defect (vacancy and interstitial). This point defect formation is the conventional source of unit cell expansion and heterogeneous microstrian in irradiated actinide dioxides. On the right side, a cation has captured an electron following relaxation of the irradiation-induced electron cascade. The resulting valence reduction from the tetravalent state to the trivalent state is accompanied by an increase in ionic radius due to enhanced screening of the nuclear charge. This redox-driven expansion causes distortion similar to that of point defect formation in actinide dioxides with cations that possess a stable trivalent state.

irradiation, Raman modes attributed to local hypo- and hyper-stoichiometric regions were observed, along with a mode characteristic of point defect accumulation.

In contrast to this detailed study of radiation effects in many fluorite-structured actinide dioxides, few investigations have focused on the sesquioxide and trioxide phases formed by some technologically-important actinides. The sesquioxides Am_2O_3 and Cm_2O_3 undergo polymorphic transformations in response to alpha particle self-irradiation (Hurtgen and Fuger, 1977; Wallmann, 1964), and similar transformations have been observed in a systematic investigation of analogue Ln_2O_3 materials (Tracy et al., 2015b). In response to irradiation with swift heavy ions of mass and energy similar to those of fission fragments, UO_3 undergoes an irradiation-induced redox reaction to form fluorite-structured UO_{2+x} (Tracy et al., 2015a).

3.2. High temperature

At ambient pressure, the fluorite structured actinide dioxides are stable up to their melting temperatures. Their thermophysical properties are generally well-understood, with some exceptions. Recent high temperature work on UO_2 has sought to explain an observed abnormal increase in the thermal expansion and heat capacity of this material starting at temperatures of approximately 1200 K (Ruello et al., 2005). The development of significant anion sublattice disorder around this temperature was identified using neutron diffraction. This behavior has been attributed to polaron formation, which has also been proposed as the source of the exceptional resistance of UO_2 to damage caused by radiation-induced thermal spikes (Desgranges et al., 2012). Other work has focused not on phase behavior, but on the high temperature processing of fuels. For example, grain growth and water desorption in nanocrystalline UO_2 have been tracked (Abril et al., 2011), and high temperature electron microscopy techniques have been developed to directly monitor sintering of nuclear fuels, in concert with conventional dilatometry measurements of densification (Clavier et al., 2013).

Advances in laser heating techniques, along with coupled XRD measurements, have recently allowed for characterization of the high temperature behavior of actinide materials with improved precision and in previously inaccessible temperature regimes. The short-range structure of liquid UO_2, at temperatures in excess of its melting point, was recently characterized for the first time using laser heating experiments (Skinner et al., 2014). X-ray total scattering techniques allowed for tracking of U-O coordination changes during the melting transition. Melting temperatures in the binary systems PuO_2-UO_2 (Böhler et al., 2014b) and ThO_2-UO_2 (Böhler et al., 2014a) have recently been reassessed, using laser heating to yield more precise measurements than previous furnace heating experiments. Finally, laser techniques have been used to clarify the influence of hyperstoichiometry on the melting temperatures of UO_{2+x} phases (Manara et al., 2005a, 2005b, 2004). These results indicate that previous determination of this relation underestimated the melting temperature decrease that accompanies increased oxygen content, again demonstrating the importance of actinide redox behavior and oxidation state variability on the phase behavior of actinide oxides in extreme environments.

Many *in situ* high temperature XRD experiments have focused on the systematic study of actinide oxide solid solutions. This is particularly important because many advanced fuel concepts aim to incorporate transuranic waste radionuclides (in the case of IMFs) or PuO_2 (in the case of MOX fuels) into conventional UO_2 fuel pellets. To better understand the processing and reactor performance of such materials, recent studies have tracked the phase evolution of binary actinide oxide systems at high temperature, monitoring structural transitions and solid state reactions. For example, phase separation upon cooling of $(U,Pu)O_2$ was investigated in this manner (Vauchy et al., 2014). It was shown that this separation can induce significant microstructural damage in the form of cracking, indicating that the integrity of MOX fuels exposed to high temperatures cannot necessarily be predicted based on the behavior of conventional UO_2 fuel pellets. Others tracked the high temperature solid-state reaction of UO_2 with AmO_2, finding that oxygen transfer between the two materials and concomitant stoichiometry changes precede the formation of a solid solution (Lebreton et al., 2012). UO_2 and AmO_2 were found to transform to U_4O_9 and Am_2O_3, prior to the formation of fluorite-structured $(U,Am)O_2$ as 1740 K. This indicates that the formation behavior of such solid solutions is closely linked to the redox behavior of actinide materials, as has also been observed for their radiation responses (Tracy et al., 2015a). Further evidence of this effect has been demonstrated by tracking of the high temperature oxidation of $(U,Np)O_2$ solid solutions (Chollet et al., 2013). It was shown that the incorporation of neptunium, which has a strong propensity to retain its tetravalent oxidation state and therefore to resist hyperstoichiometry, inhibits the formation of U_4O_9 and U_3O_8 phases. From these results, it is clear that the variability in stable electronic configurations exhibited by the light actinide elements can have a significant effect on the behavior of actinide oxides at high temperatures.

3.3. High pressure

Starting at pressures of approximately 30–40 GPa, most fluorite-structured actinide oxides undergo a sluggish

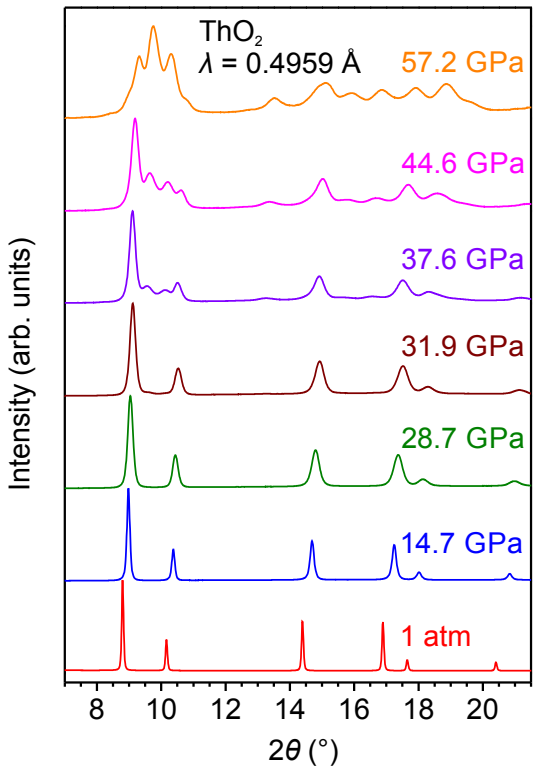

Fig. 4. XRD patterns of ThO_2 as a function of pressure at ambient temperature. At 31.9 GPa, a transformation to a cotunnite-like phase is observed, finishing by 57.2 GPa. Patterns were measured in transmission mode on a DAC-loaded sample.

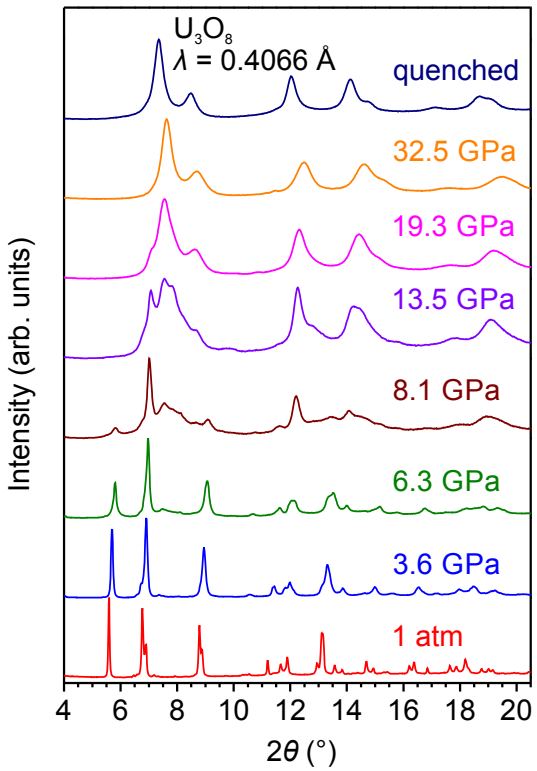

Fig. 5. XRD patterns of α-U_3O_8 as a function of pressure at ambient temperature. Starting at 8.1 GPa, a transformation to a cubic fluorite-like phase is observed, along with partial amorphization as indicated by the presence of broad bands resulting from diffuse scattering. This data is reported in detail in (Zhang et al., 2014b).

transformation to a cotunnite-like phase (*Pnma*), with the exception of NpO_2, which instead transforms to an orthorhombic phase (*Cmcm*) (Benedict et al., 1992; Idiri et al., 2004). This high pressure behavior has been demonstrated by both XRD (Idiri et al., 2004) and Raman spectroscopy measurements (Jayaraman et al., 1988). Fig. 4 shows XRD patterns of ThO_2 as a function of pressure, illustrating the transformation. Few reports of shock compression of actinide oxides has been reported in the literature, yet a polymorphic phase transformation at approximately 50 GPa has been observed under transient loading conditions at ambient temperature (Molodets and Fortov, 2004). The structure of the phase formed in these experiments was not determined.

Recent results have shown that deviation from the ideal dioxide stoichiometry can significantly influence the high pressure polymorphism of the actinide dioxides. A $(Th_{0.71},U_{0.31})O_{2.09}$ solid solution was found to transform to a phase isostructural with tetragonal ZrO_2 at a relatively low pressure of 3 GPa (Tschauner et al., 2013), in contrast to the higher pressure transformation to cotunnite observed in stoichiometric UO_2 and ThO_2. Pressurization of orthorhombic α-U_3O_8 causes its transformation to a cubic phase with a structure similar to fluorite (Zhang et al., 2014b). Refinement of XRD patterns collected from this high pressure phase indicate an ideal fluorite face-centered cubic cation arrangement, yet a modified anion sublattice due to the presence of adventitious oxygen, such that the phase can be described as UO_{2+x}. This transformation is illustrated in Fig. 5, which shows XRD patterns of α-U_3O_8 as a function of pressure. Unlike the cotunnite high pressure phase of the stoichiometric actinide dioxides, this cubic high pressure phase can be recovered to ambient conditions. Because of the chemical complexity common to the actinides, nonstoichiometry and mixed valence state compounds are common, as demonstrated by the prevalence UO_{2+x} and PuO_{2-x} phases. Therefore, to better predict the behavior of actinide oxide nuclear materials in the extreme environments in which they operate, systematic study of the effects of nonstoichiometry on high pressure phase transformations is necessary.

3.4. Combined extreme conditions

Limited information on the behavior of binary actinide oxides under combined irradiation, temperature, and pressure is available in the literature, yet the results that have been reported show interesting effects. High temperature studies of pre-irradiated materials have been used to investigate the annealing of radiation-induced defects. Such work has been performed for UO_2 irradiated with fission fragments (Nakae et al., 1978a), and for CeO_2 and ThO_2 irradiated with swift heavy ions (Palomares et al., 2015). UO_2 and CeO_2 both exhibited multi-stage defect recovery as a function of annealing temperature, as indicated by multiple relatively abrupt changes in lattice parameter during heating. This suggests the presence of multiple modes of damage (*e.g.*, cation vacancies, anion interstitials, etc.). Some of these modes might be related to local stoichiometry or redox changes in these materials, which contain cations that are susceptible to ionization-induced redox changes. In contrast, redox-resistant ThO_2 showed only a single recovery stage. Thermal recovery following alpha particle irradiation of CeO_2, PuO_2, and UO_2 was studied in a similar manner (Weber, 1984, 1983; Wiss et al., 2014). For all three materials, multi-stage recovery was observed. The activation energies of defect recovery were shown to vary strongly between materials. It is interesting to note that damage in UO_2 recovers more efficiently than that of PuO_2, despite the finding, discussed above in Section 3.1, that PuO_2 is more resistant to alpha radiation-induced unit cell

expansion. This suggests that the radiation tolerance of these materials may be controlled by the mobility of their constituent atoms, which governs the energy needed for their displacement. In this way, annealing studies complement direct characterization of the damage resulting from irradiation, offering further insight into the types of defect produced and the mechanisms of defect production or annihilation.

Alongside post-irradiation annealing studies, heating of a sample during irradiation can simulate the radiation response of a fuel pellet in the high temperature environments characteristic of reactor operation conditions. Generally, an increase in the temperature at which irradiation is performed leads to a reduction of radiation damage due to enhanced defect recovery. For example, an inverse proportionality between irradiation temperature and simulated fission fragment track diameter has been demonstrated in the nuclear fuel analogue CeO_2 (Sonoda et al., 2006). However, few such studies have been performed to date.

No studies of the high pressure behavior of irradiated fluorite materials, or of the effects of pressure on the radiation responses of such materials, have been reported. However, the influence of ionizing radiation on the high pressure behavior of ZrO_2, which has a high temperature fluorite-structured polymorph, has been studied. Irradiation of this material at ambient conditions induces a transformation from its ambient-temperature monoclinic phase ($P2_1/c$) to the intermediate-temperature tetragonal polymorph ($P4_2/nmc$) (Benyagoub, 2005; Benyagoub et al., 2001). When irradiated with swift heavy ions at high pressures of up to 14 GPa, a transformation to the high-temperature fluorite polymorph was instead observed (Schuster et al., 2012). Upon quenching to ambient conditions, this material underwent a transition to the tetragonal polymorph. In this way, the tetragonal phase was produced using ion fluences much lower than those required to induce the transformation without the simultaneous application of pressure (Schuster et al., 2009). When irradiated at 23 GPa, at which point it exhibits an orthorhombic *Pbca* high pressure phase, ZrO_2 undergoes a second radiation-induced phase transformation to another orthorhombic phase that is, in the absence of radiation, stable only above 30 GPa (Schuster et al., 2012). These results suggest that the rapid, localized deposition of energy by highly-ionizing radiation can make accessible new high pressure phase transition pathways, and that radiation exposure may be an important factor when considering the phase space of nuclear materials. Thus, similar studies of actinide oxides are needed to better understand how such materials would respond to irradiation in, for example, high pressure geological disposal conditions.

The simultaneous exposure of a material to high temperature and high pressure can be used to explore its phase space, which is crucial for many nuclear applications where materials might encounter mechanical stresses, high temperatures, and steep thermal gradients. Studies of the pressure dependence of the melting temperature of UO_2 have shown proportionality between the two up to 250 MPa, with the melting temperature increasing by approximately 100 K/GPa (Manara et al., 2005b, 2002). The high temperature behavior of the previously discussed (Section 3.3) high pressure, fluorite-like phase of α-U_3O_8 has been studied by laser heating of the material at 38 GPa and up to 1700 K (Zhang et al., 2014b). Exceptional stability of this phase was observed. As shown in Fig. 6, it maintained its cubic structure under these conditions. Similar work has been performed on CeO_2, ThO_2, and UO2 (Liu, 1980). This laser heating study of actinide oxides in a DAC found that, after quenching from 10 GPa and around 1100–1300 K to ambient conditions, ThO_2 transformed to an orthorhombic phase with a structure similar to that of Ni_2Si, but distinct from the ambient temperature, high pressure cotunnite phase. No changes were observed in the other compounds. In this study, XRD patterns were collected only after quenching, so the *in situ* phase behavior of the material is unknown.

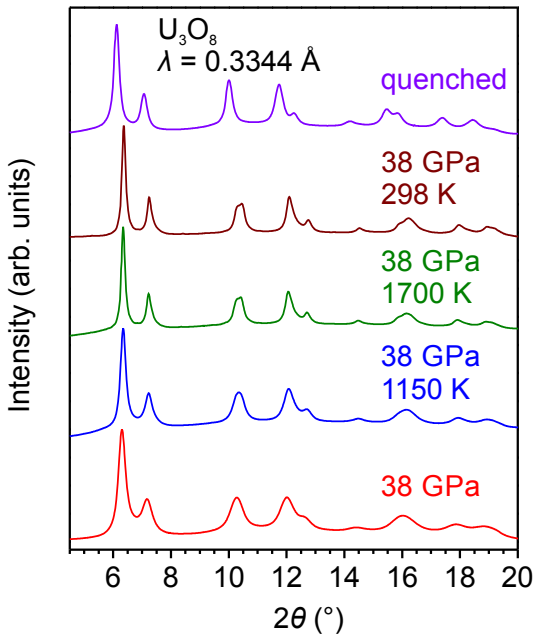

Fig. 6. XRD patterns of the high pressure, fluorite-like phase of U_3O_8 exposed to simultaneous high pressure and high temperature. Under all conditions tested, this phase retains its structure. Measurements were made using laser heating of material loaded in a DAC, and are reported in detail in (Zhang et al., 2014b).

More recent experiments on pressurized natural UO_2 at 2000 K showed two transformations with increasing pressure (Greaux et al., 2008). The first occurred below 18 GPa and involved a minor modification of the initial fluorite phase, producing a pyrite-like structure (*Pa*-3). This phase possesses the same cation sublattice as the fluorite structure, but a modified anion sublattice. This is similar to the structure of the UO_{2+x} high pressure phase of α-U_3O_8 discussed in Section 3.3 (Zhang et al., 2014b). This similarity is particularly interesting in consideration of the fact that natural uranium dioxide, as reported here, is generally hyper-stoichiometric. At higher pressures, a transformation from the pyrite-like phase to one isostructural with the high pressure orthorhombic *Pbca* phase of ZrO_2 was observed (Greaux et al., 2008). In both these cases, phase transformations distinct from those known to occur at ambient temperature were observed. However, this study made use of natural uranium dioxide, for which nonstoichiometry and impurities can significantly influence pressure and temperature response. Recent systematic study of the high pressure behavior of ThO_2 and UO_2 at temperatures between 1900 K and 2500 K found only a transformation to the cotunnite-like phase at pressures of up to 65 GPa (Chidester et al., 2013). These results suggest that small changes in the stoichiometry of uranium oxides can change the high pressure phase space, a phenomenon that is not expected to occur for ThO_2, for which non-stoichiometry is not observed. Clearly, more systematic work on well-characterized materials is necessary to map their pressure-temperature phase space and to better distinguish between the effects of temperature and nonstoichiometry on high pressure phase transformations.

4. Results for complex oxides

Complex oxides are found in the nuclear fuel cycle primarily as actinide-bearing minerals and proposed waste management

materials (Ewing, 2011). The latter class of materials, which includes both wasteforms and IMFs, are often designed to mimic the behavior of actinide-bearing minerals that are known to retain their structures and properties following long-term radiation exposure (Ewing, 2007; Ewing et al., 2004, 2000; Lumpkin, 2001). Study of the behavior of these complex oxides in extreme environments is needed to ensure adequate performance of such materials in reactor or repository conditions. These investigations can also yield insight into the environmental behavior of actinide materials, including both ores and materials formed following reactor accidents (Burns et al., 2012; Ewing, 2011). Recently, a great deal of work has focused on $A_2B_2O_7$ materials with the pyrochlore structure (*Fd*-3*m*) (Subramanian et al., 1983), as they exhibit favorable radiation tolerance and resistance to radionuclide leaching, while also easily incorporating actinides (Ewing, 2011; Ewing et al., 2004). In these materials, the A-site is typically occupied by a large cation, such as a lanthanide or actinide, while the B-site is occupied by a smaller transition metal or group 14 element. Much of the work discussed in this section focuses on the study of lanthanide-bearing complex oxides, which can serve as useful analogues for actinide-bearing materials given the similarities of the lanthanide and actinide elements.

4.1. Ionizing radiation

Complex oxides tend to have highly-ordered structures that do not easily incorporate defects in high concentrations. Thus, radiation-induced atomic displacement often causes them to amorphize or undergo an order-disorder transformation into a defect-rich phase with a less complex structure. Amorphization can impair the ability of a material to effectively contain actinides, increasing leach rates and facilitating the environmental release of radionuclides (Ewing et al., 2004; Laverov et al., 2009). Thus, materials which maintain crystallinity under exposure to ionizing radiation are particularly well suited for use as wasteforms and IMFs. Pyrochlore materials exhibit a unique radiation-induced disordering process wherein the formation of cation antisite defects and anion Frenkel pairs leads to a decrease in the symmetry of the material's structure to that of the fluorite structure (*i.e.* from *Fd*-3*m* to *Fm*-3*m*) (Sickafus et al., 2000). In pyrochlores for which cation antisite defects are not stable due to a large size mismatch between A- and B-site cations, amorphization occurs instead of this disordering. Therefore, the radiation tolerance of pyrochlore materials can be tailored by control of their composition, with tolerance increasing as the value of the cation ionic radius ratio, r_A/r_B, decreases (Lang et al., 2014, 2010, 2009a, 2009b; Sattonnay et al., 2012, 2010). To illustrate this effect, Fig. 7 shows high-resolution TEM micrographs of ion tracks in $Gd_2Ti_{2-x}Zr_xO_7$ compounds irradiated with swift heavy ions. $Gd_2Ti_2O_7$, which has a large r_A/r_B, exhibits a large, fully amorphous ion tracks. The amorphous in-track structure is indicated by the aperiodic “speckle” contrast within the track area. In contrast, $Gd_2Zr_2O_7$, which has a larger B-site cation and hence a smaller r_A/r_B, exhibits no amorphous material within its ion tracks. This highly radiation tolerant material only exhibits disordering and defect formation in response to energy deposition by a swift heavy ion. Gd_2TiZrO_7, which has an intermediate average r_A/r_B, shows mixed behavior, with a disordered annular track shell surrounding an amorphous cylindrical track core. XRD data shown in Fig. 7, collected from these three materials following irradiation to various ion fluences, corroborates the TEM observations. With increasing fluence, $Gd_2Ti_2O_7$ adopts an amorphous structure, $Gd_2Zr_2O_7$ loses its pyrochlore superstructure but retains fluorite-like ordering, and Gd_2TiZrO_7 shows a mixed response of simultaneous disordering and amorphization.

As is crucial for the design of nuclear components based on these materials, this disordering mechanism has recently been demonstrated for actinide-bearing pyrochlores. XRD characterization of self-irradiated $Am_2Zr_2O_7$ (Belin et al., 2009; Martin et al., 2009; Sykora et al., 2005) and $Cf_2Zr_2O_7$ (Sykora et al., 2005) has shown a transformation of these materials, over time, to fluorite-structured phases. Leaching studies have demonstrated increased actinide release by amorphized pyrochlore materials during contact with water, but little change compared to pre-irradiation performance in those that disorder to fluorite (Ewing et al., 2004; Laverov et al., 2009). Thus, $An_2Zr_2O_7$ pyrochlores, which resist amorphization, are viable waste forms that can effectively immobilize actinides despite radiation exposure due to alpha decay and the spontaneous fission of actinides. This radiation tolerance is unique, as many complex oxides amorphize when exposed to ionizing radiation. Irradiation-induced amorphization has been demonstrated for the actinide-bearing materials soddyite $(UO_2)_2(SiO_4)(H_2O)_2$ (Sureda et al., 2011), uranophane $Ca(UO_2)_2(SiO_3OH)_2(H_2O)_5$ (Sureda et al., 2011; Utsunomiya et al., 2003), and both zircon- and scheelite-structured $ThGeO_4$ (Patel et al., 2010), along with proposed wasteforms such as perovskite $CaZrO_3$ (Lang et al., 2012), garnet $Y_{2.89}Cm_{0.1}Pu_{0.01}Al_5O_{12}$ (Livshits et al., 2010), apatite $Ca_{10}(PO_4)_6(OH,F,Cl)_2$ (Afra et al., 2011; Liu et al., 2008; Miro et al., 2011, 2005; Weikusat et al., 2010), and pyrochlore-like orthorhombic A_2TiO_5 (Tracy et al., 2012).

4.2. High temperature

Many complex oxides phases incorporate actinides, including approximately five percent of all known minerals (Finch and Murakami, 1999). This diversity yields a wide variety of high temperature polymorphic phase transformations. This review focuses on the behavior of materials with the pyrochlore structure which, as discussed in Section 4.1 of this review, are good candidates for use in IMF and wasteform nuclear components. Many pyrochlore compositions exhibit a high temperature transformation to a disordered fluorite phase. This process is analogous to the order-disorder transformation induced by irradiation, and a trend of decreasing transition temperature with decreasing r_A/r_B is evident (Wuensch et al., 2000). This trend is due to the improved energetics of cation antisite formation with A- and B-site cations of similar ionic radius, as formation of these defects is necessary for the disordering process to occur. Because transformation to a fluorite phase does not substantially inhibit the ability of pyrochlore materials to immobilize actinides, this high temperature phase behavior is not likely to adversely affect the performance of synthetic wasteforms or IMFs.

While the structural effects of high temperature exposure are of minor concern for the use of these materials in nuclear applications, its effects on the chemistry of actinide materials can be substantial. Many actinide elements have highly variable redox behavior and readily change oxidation state. Americium in $Am_2Zr_2O_7$ compounds can oxidize from its initial trivalent state to a tetravalent state, concomitant with the uptake of oxygen from the material's environment. However, high temperature XRD measurements in oxidizing atmospheres (Otobe et al., 2011) have shown that the pyrochlore structure is maintained despite such oxidation. The structural and chemical flexibility of the pyrochlore system, which is known to incorporate aliovalent cations (divalent, trivalent, tetravalent, and pentavalent) (Subramanian et al., 1983) is particularly well suited to the containment of actinides, for which valence changes under extreme conditions are likely. This further demonstrates the unique ability of pyrochlore materials to maintain their structures, and therefore properties, in extreme environments.

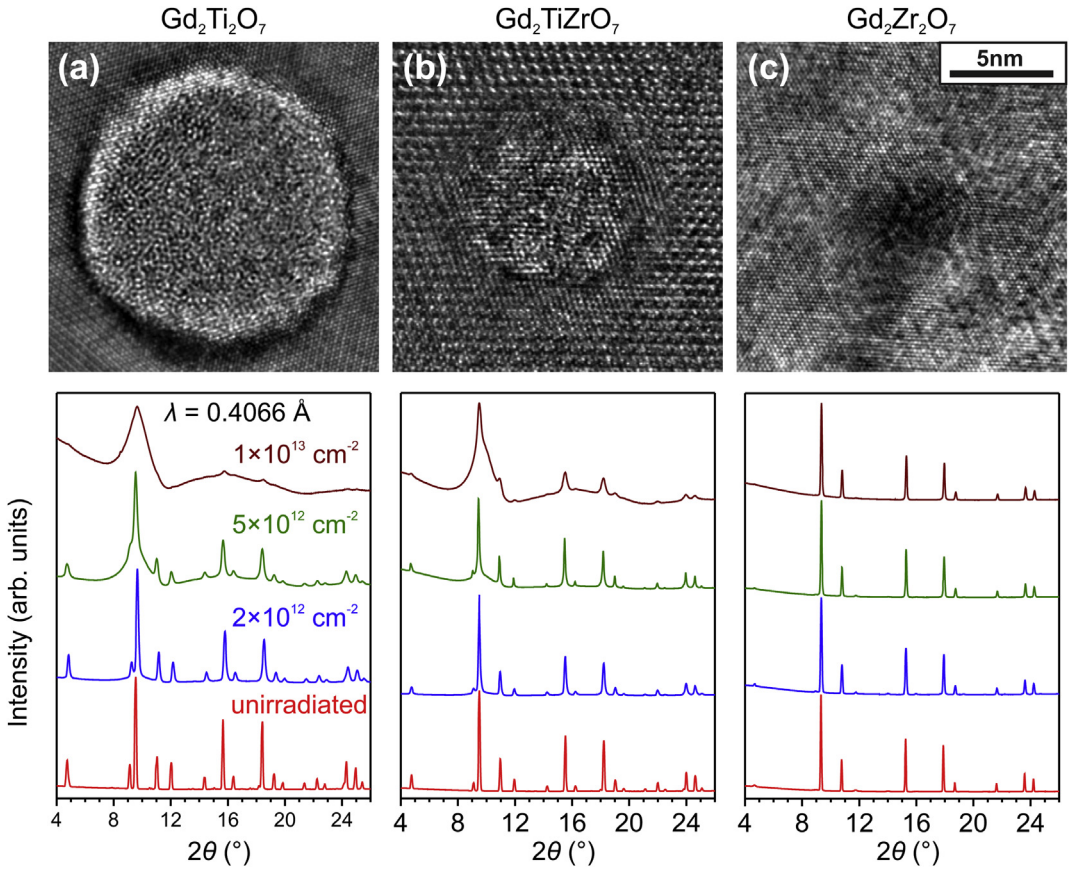

Fig. 7. TEM and XRD data from various compositions of $Gd_2Ti_{2-x}Zr_xO_7$ irradiated with swift heavy ions. As the zirconium content of these materials is increased, less amorphization per incident ion is observed and the extent of disordering by irradiation increases. Amorphization is indicated by the in-track "speckle" contrast in the TEM micrographs and by the broad, diffuse scattering features in the XRD patterns. Disordering to the defect fluorite structure is indicated by the loss of some periodic superstructure features in the TEM micrographs and by attenuation of weak superstructure diffraction maxima in the XRD patterns. In (b) a disordered annular track shell surrounds an amorphous cylindrical track core in the compound Gd_2TiZrO_7. TEM micrographs are shown for irradiation with 2.2 GeV Au ions, from (Lang et al., 2014), while XRD patterns are shown for irradiation with 1.4 GeV Xe ions, from (Lang et al., 2009b).

4.3. High pressure

Like simple oxides with the fluorite structure, many pyrochlore compounds have been shown to transform to a cotunnite-like phase at high pressure (Lang et al., 2010; Xiao et al., 2010). This is often followed by either amorphization or disordering to a defect fluorite phase during quenching to ambient conditions. As with their responses to irradiation and high temperature, this behavior is dependent on the pyrochlore cation ionic radius ratio, r_A/r_B. The critical pressure for the pyrochlore-to-cotunnite transformation is proportional to this cation radius ratio, as is the propensity of such materials to amorphize, rather than disordering to fluorite, upon pressure quenching. Thus, while pyrochlores with small r_A/r_B values are typically resistant to amorphization by irradiation and pressure quenching, they tend to be more susceptible than those with higher cation radius ratios to high pressure phase modification. Comparative high pressure XRD patterns from $Gd_2Ti_2O_7$ and $Gd_2Zr_2O_7$ are shown in Fig. 8, illustrating the differing stability ranges of the pyrochlore phase. The high pressure transformation of pyrochlore compounds to the cotunnite-like phase has recently been demonstrated for actinide-bearing materials. Fig. 9 shows XRD evidence of the transformation in $Gd_{1.8}U_{0.2}Zr_2O_7$ (Zhang et al., 2014a).

Due to the utility of high pressure research from a mineralogy perspective, extensive work has been performed on various other complex oxides, including many actinide materials. For example, $ThTi_2O_6$ and $Y_{0.5}U_{0.5}Ti_{1.5}Nb_{0.5}O_6$, both exhibiting the brannerite structure, have been studied with XRD, Raman spectroscopy, and IR absorption techniques (Zhang et al., 2011a,b). In contrast to the pyrochlores, these compounds begin to amorphize at relatively low pressures around 20 GPa $ThGeO_4$, which can adopt either zircon or scheelite structures at ambient conditions, follow a sequential high pressure transformation path in which the zircon phase transforms to a scheelite structure, which then transforms at higher pressures to a fergusonite structure (Errandonea et al., 2009). Both of the latter two high pressure phases quench to scheelite. Coffinite $USiO_4$, which also exhibits a zircon structure, undergoes the same high pressure transformation to a scheelite phase at around 15 GPa, but a second transformation to fergusonite has not been observed up to 45 GPa, although partial amorphization was observed at this pressure (Zhang et al., 2009). Interestingly, IR spectroscopy measurements suggest that the transformation to the scheelite phase might be accompanied by a change in the oxidation state of uranium from tetravalent to the rare pentavalent state. In comparison, zircon-structured $ZrSiO_4$ transforms to the scheelite structure at approximately 23 GPa, at room temperature (Knittle, 1993). This critical transformation pressure decreases to 12 GPa at 1273 K (Liu, 1979), suggesting that the transformation may show temperature dependence in the zircon-structured actinide oxides. Comparative study of the high pressure transformations of isostructural $USiO_4$ and $ZrSiO_4$ might elucidate the role of uranium oxidation state changes, as zirconium cannot be oxidized beyond the tetravalent state, while uranium can.

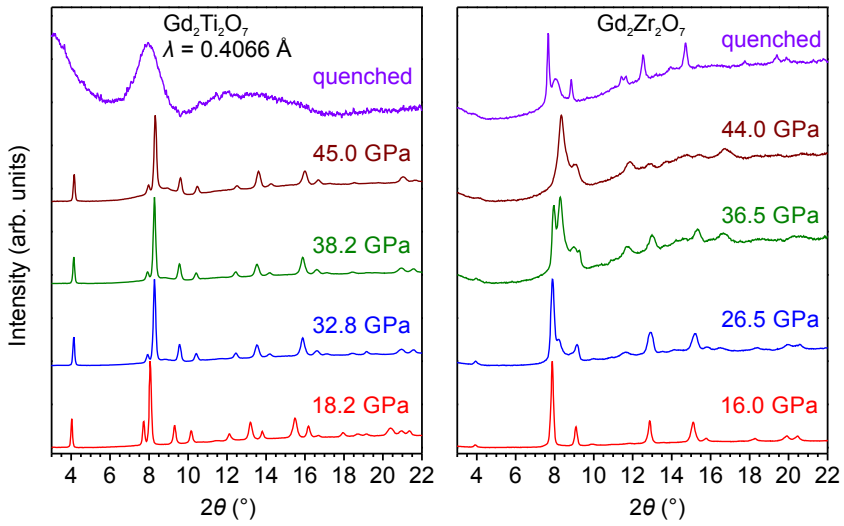

Fig. 8. XRD patterns of $Gd_2Ti_2O_7$ (left) and $Gd_2Zr_2O_7$ (right) as a function of pressure, at ambient temperature. Both materials initially exhibit the pyrochlore structure, but transform to the cotunnite-like phase with increasing pressure. This transformation is complete for the zirconate compound by 44 GPa, while the titanate compound remains predominantly pyrochlore at this pressure. From the high pressure phase, the titanate compound quenches to an amorphous phase, while the zirconate quenches to a defect fluorite phase. This data is adapted from (Zhang et al., 2008).

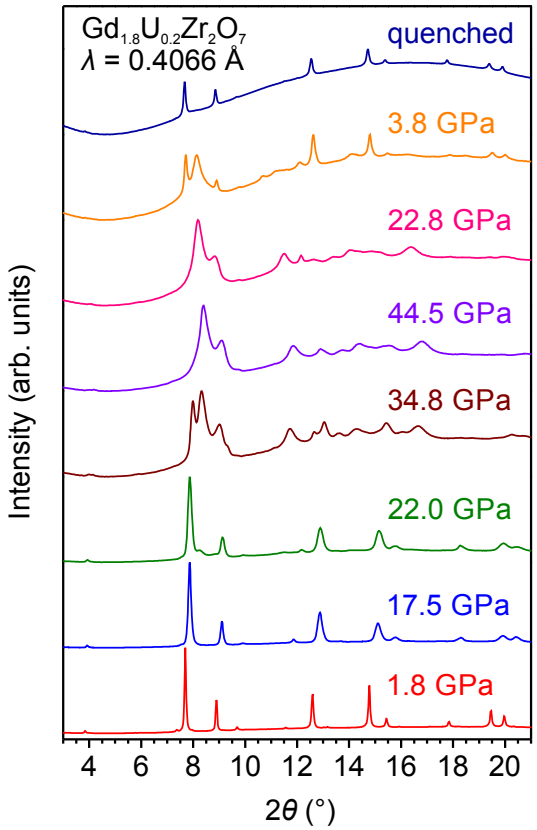

Fig. 9. XRD patterns of $Gd_{1.8}U_{0.2}Zr_2O_7$ as a function of pressure at ambient temperature. Starting at 22 GPa, a transformation to a cotunnite-like phase is observed. Upon quenching to ambient pressure, the sample recovers a defect fluorite structure. This data is adapted from (Zhang et al., 2014a).

4.4. Combined extreme conditions

Few actinide-bearing complex oxides have been investigated under combined irradiation, high temperature, and/or high pressure. Nonetheless, some studies have shown interesting behavior under these conditions. Electron irradiation at high temperature has been performed for both soddyite $(UO_2)_2(SiO_4)(H_2O)_2$ and uranophane $Ca(UO_2)_2(SiO_3OH)_2(H_2O)$ (Sureda et al., 2011). As was the case for irradiation of fluorite simple oxides, discussed above in Section 3.1, increased irradiation temperature resulted in decreased damage as a function of radiation fluence. For these complex oxides, this was evidenced by an increase in the radiation fluence necessary for amorphization. Investigation of the critical temperature for amorphization of actinide pyrochlore compounds, meaning the temperature above which amorphization will not occur, has been performed using low velocity ions, for which elastic nuclear collisions between nuclei dominates the energy transfer (Ewing et al., 2004). However, similar data on their response to ionizing radiation is not available in the literature. The same is true of post-irradiation annealing investigations, which have been extensively reported for displacive irradiations (Ewing et al., 2004), but never for the high specific energy regime of radiation. Because both wasteforms and IMFs will operate at temperatures above ambient due to radionuclide decay and fission heating (estimated to be around 300–550 K for repository conditions (Ewing et al., 2004) and on the order of 1000 K for reactor conditions), high temperature irradiation studies are necessary for prediction of the behavior of these nuclear materials in fuel cycle applications.

For other complex oxides, limited data on swift heavy ion track annealing have been reported. Shrinkage in the diameter of ion tracks in apatite as a function of temperature has been tracked using SAXS (Afra et al., 2011). This yielded insight into the precise mechanisms of damage recovery, as it allowed for the construction of Arrhenius plots to determine the activation energies of damage recovery processes. This is similar to the technique discussed in Section 3.1 of this review, wherein XRD characterization of the annealing of alpha particle irradiation-induced unit cell expansion in fluorite oxides was used to determine defect recovery activation energies (Weber, 1984). TEM characterization of ion tracks in apatite has been performed to directly observe track shrinkage via vacancy emission from the interior of ion tracks, leading to reduction in the in-track density (Li et al., 2011). Again, this is analogous to the aforementioned STEM work on CeO_2 (Takaki et al., 2014), which found that ion tracks in this material exhibited

reduced atomic density. Finally, post-irradiation annealing of lanthanide-bearing pyrochlores that have been amorphized by swift heavy ion irradiation have shown that the temperature at which the pyrochlore phase recrystallizes depends strongly on the ionic radius of the lanthanide cation (Park et al., 2015). This suggests that similar compositional variation might occur in actinide-bearing pyrochlores, due to the analogous ionic radius contraction across the actinide series.

Novel effects of high pressure irradiation on the phase behavior of compounds isostructural with actinide-bearing materials have recently been reported. A study of the response of pyrochlore-structured $Gd_2Zr_2O_7$ to swift heavy ion irradiation at high pressure has shown the stabilization of a new phase of this material to ambient conditions (Lang et al., 2009d). After irradiation of this compound's cottunite phase at high pressure, quenching of the material to ambient conditions yielded an *Im*-3*m* body-centered cubic phase isostructural with the high temperature cubic phase of Gd_2O_3. This process, which is illustrated in Fig. 10, was attributed to the effect of a nanocrystalline microstructure produced by irradiation, which modified the phase stability of the material due to interface effects. Further evidence of radiation-induced phase destabilization at high pressure has been reported for zircon $ZrSiO_4$, for which a transformation to the high pressure reidite phase, with the scheelite structure, was induced well below the normal critical pressure for this transformation of approximately 23 GPa (Lang et al., 2009c). In contrast to this *in situ* irradiation of complex oxides at high pressure, which tends to destabilize ambient pressure phases, the pressurization of pre-irradiated materials has been shown to increase the pressure needed to induce high pressure polymorphic transformations. Zircon irradiated prior to pressurization did not exhibit a transformation to the reidite phase up to 36 GPa (Lang et al., 2009c). Raman characterization of apatite yielded a similar finding, with pre-irradiated material showing increased resistance to pressure-induced amorphization (Liu et al., 2008; Weikusat et al., 2010). These studies used intermediate ion irradiation fluences, such that defects were induced in the materials tested but complete radiation-induced amorphization was not achieved. Study of zircon that has been amorphized by exposure to alpha irradiation has been performed, and observation of an abrupt increase in density and softening of the material was attributed to an amorphous-to-amorphous phase transformation at approximately 4.5 GPa (Trachenko et al., 2007). The relation of irradiation to the high pressure phase behavior of materials with the zircon structure may be important for the mineralogy of isostructural actinide-bearing phases, such as coffinite $USiO_4$. These natural materials will typically experience significant exposure to fission fragment and alpha particle irradiation due to the presence of actinide elements. However, no experiments have been performed on these systems thus far.

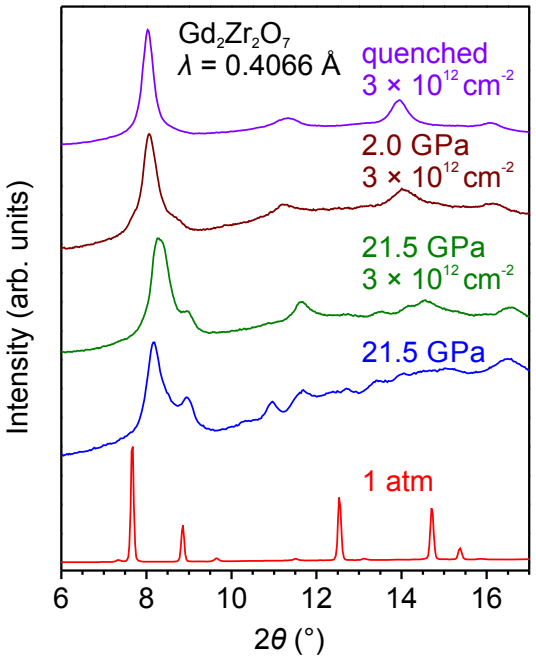

Fig. 10. XRD patterns of $Gd_2Zr_2O_7$ brought to pressures above the pyrochlore-to-cotunnite critical transition pressure at ambient temperature, then irradiated with 7 GeV U ions to a fluence of 3×10^{12} cm^{-2} and quenched back to ambient pressure. Under these processing conditions, a non-fluorite cubic phase isostructural with the high temperature polymorph of Gd_2O_3 was recovered. This data is adapted from (Lang et al., 2009d).

While high temperature-high pressure studies have been performed on numerous earth materials, little work has been performed on complex oxides of relevance to nuclear energy. However, a single study has investigated the behavior of zircon exposed to high temperatures and pressures characteristic of the conditions in Earth's crust (0.75 GPa and 523 K), along with *in situ* irradiation with swift heavy ions (Lang et al., 2009c, 2008). This advanced extreme environment study showed that, in these conditions, the diameter of simulated fission fragment ion tracks was increased compared to those formed at ambient pressure and temperature. Based on this demonstration of a technique for such measurements, future studies of actinide-bearing materials might allow for accurate assessment of the behavior of nuclear wasteforms in geological disposal conditions.

5. Conclusions

From the numerous studies described here, it is clear that oxides relevant to nuclear energy exhibit diverse structural and chemical responses to extreme environments. This behavior is further complicated by the influence of radiation-induced defects on the high pressure-high temperature behavior of these materials, along with the pressure and temperature dependence of radiation-induced defect production. These extreme conditions, when applied either individually or simultaneously, can cause dramatic modifications to actinide oxides that greatly affect their properties and, therefore, their performance in nuclear applications. However, the literature reporting studies of actinide-bearing materials under such conditions is limited and, in many cases, not sufficient for meaningful application to fuel cycle issues. For example, minor hyperstoichiometry in UO_2 has been shown to result in transformations under combined high pressure and temperature that differ from those of the stoichiometric phase (Greaux et al., 2008). However, only a single UO_{2+x} phase has been investigated in this manner, so general conclusions regarding the influence of adventitious oxygen on the behavior of this material in extreme environments cannot be made. Furthermore, the data available is often not directly comparable, due to differences in sample type and experimental methods, such as variation in sample stoichiometries or irradiation energies. Finally, many of the interesting behaviors observed in materials that are isostructural with technologically-important nuclear fuel cycle materials (*e.g.*, zircon, lanthanide bearing pyrochlores, and lanthanide sesquioxides) suggest that similar behaviors might exist for actinide-bearing materials, but few attempts have been made to confirm these suggestions. If experiments in this area are to be applied to the design or assessment of nuclear fuel cycle materials, additional targeted, systematic investigation is required.

It is also clear, based on the work reviewed here, that solid-state

redox chemistry is a crucial factor in the phase behavior of actinide materials under extreme conditions. The light actinide elements possess partially-itinerant *f*-electrons and, therefore, significant variation in stable electronic configurations (Krupa, 2005). This leads to diverse solid state chemistry, in terms of both *f*-orbital occupancy and redox behavior, resulting in diverse responses to extreme conditions among otherwise similar, isostructural materials. For example, ThO_2 and UO_2 were shown to exhibit dramatic differences in the rate of ionizing radiation-induced damage accumulation, possibly due to the presence of 5*f* orbital traps for excited electrons in the latter material (Figs. 2 and 3). Similarly, the high pressure phase space of UO_{2+x} has been found to vary dramatically as a function of oxygen content, in contrast to ThO_2 which does not exhibit nonstoichiometry (Sections 3.3 and 3.4). The doping of UO_2 with other actinide elements that exhibit differing redox behavior, such as neptunium, suppresses the material's oxidation-induced high temperature phase evolution to U_3O_8 (Section 3.2). The addition of the actinide element americium to pyrochlore compounds leads to oxidation changes that can cause deviations in the high temperature behaviors of these materials, as compared with lanthanide-bearing pyrochlores (Section 4.2). Because of this complex compositional variation in phase behavior, the response of a specific actinide oxide material to extreme conditions often cannot be generalized to the behavior of other actinide oxide systems, despite structural similarity. The response of UO_2 to irradiation, temperature, or pressure may differ dramatically from the response of the same material with minor transuranic impurities, as is common of nuclear fuels due to transmutation. Therefore, the application of such studies to the development of nuclear fuel cycle materials requires that the precise composition of the actinide oxide component of interest be determined and accurately simulated. This also necessitates systematic study of compositional effects on extreme environment phase behavior.

Acknowledgements

This work was supported by the Energy Frontier Research Center *Materials Science of Actinides* funded by the U.S. Department of Energy (DOE), Office of Science, Office of Basic Energy Sciences (Grant No. DE-SC0001089).

References

Abdelouas, A., 2006. Uranium mill tailings: geochemistry, mineralogy, and environmental impact. Elements 335–342. http://dx.doi.org/10.2113/gselements.2.6.335.

Abril, R.J., Eloirdi, R., Bouëxière, D., Malmbeck, R., Spino, J., 2011. In situ high temperature X-ray diffraction study of UO_2 nanoparticles. J. Mater. Sci. 46, 7247–7252. http://dx.doi.org/10.1007/s10853-011-5684-4.

Afra, B., Lang, M., Rodriguez, M., Zhang, J., 2011. Annealing kinetics of latent particle tracks in Durango apatite. Phys. Rev. B 83, 064116. http://dx.doi.org/10.1103/PhysRevB.83.064116.

Baldini, M., Yang, W., Aquilanti, G., Zhang, L., Ding, Y., Pascarelli, S., Mao, W.L., 2011. High-pressure EXAFS measurements of crystalline Ge using nanocrystalline diamond anvils. Phys. Rev. B 84, 014111. http://dx.doi.org/10.1103/PhysRevB.84.014111.

Bassett, W., Shen, A., Bucknam, M., Chou, I., 1993. A new diamond anvil cell for hydrothermal studies to 2.5 GPa and from 190 to 1200 °C. Rev. Sci. Instrum. 64, 2340–2345. http://dx.doi.org/10.1063/1.1143931.

Belin, R.C., Martin, P.M., Valenza, P.J., Scheinost, A.C., 2009. Experimental insight into the radiation resistance of zirconia-based americium ceramics. Inorg. Chem. 48, 5376–5381. http://dx.doi.org/10.1021/ic900369b.

Benedict, U., Dabos-Seignon, S., Dancausse, J.P., Gensini, M., Gering, E., Heathman, S., Luo, H., Olsen, J.S., Gerward, L., Haire, R.G., 1992. Actinide compounds under pressure. J. Alloys Comp. 181, 1–12. http://dx.doi.org/10.1016/0925-8388(92)90292-H.

Benyagoub, A., 2005. Mechanism of the monoclinic-to-tetragonal phase transition induced in zirconia and hafnia by swift heavy ions. Phys. Rev. B 72, 094114. http://dx.doi.org/10.1103/PhysRevB.72.094114.

Benyagoub, A., Couvreur, F., Bouffard, S., Levesque, F., Dufour, C., Paumier, E., 2001. Phase transformation induced in pure zirconia by high energy heavy ion irradiation. Nucl. Instrum. Methods B 175-177, 417–421. http://dx.doi.org/10.1016/S0168-583X(00)00609-1.

Boehler, R., Chopelas, A., 1991. A new approach to laser heating in high pressure mineral physics. Geophys. Res. Lett. 18, 1147–1150. http://dx.doi.org/10.1029/91GL01144.

Böhler, R., Quaini, A., Capriotti, L., Çakır, P., Beneš, O., Boboridis, K., Guiot, A., Luzzi, L., Konings, R.J.M., Manara, D., 2014a. The solidification behaviour of the UO_2–ThO_2 system in a laser heating study. J. Alloys Comp. 616, 5–13. http://dx.doi.org/10.1016/j.jallcom.2014.07.055.

Böhler, R., Welland, M.J., Prieur, D., Cakir, P., Vitova, T., Pruessmann, T., Pidchenko, I., Hennig, C., Guéneau, C., Konings, R.J.M., Manara, D., 2014b. Recent advances in the study of the UO_2–PuO_2 phase diagram at high temperatures. J. Nucl. Mater 448, 330–339. http://dx.doi.org/10.1016/j.jnucmat.2014.02.029.

Burns, P.C., Ewing, R.C., Navrotsky, A., 2012. Nuclear fuel in a reactor accident. Science 335, 1184–1188. http://dx.doi.org/10.1126/science.1211285.

Cappia, F., Jovani-Abril, R., Spino, J., Luzzi, L., Janßen, A., Manara, D., 2014. Laser melting of nano-crystalline uranium dioxide. Prog. Nucl. Energy 72, 11–16. http://dx.doi.org/10.1016/j.pnucene.2013.10.018.

Chidester, B., Campbell, A.J., Fischer, R.A., Reaman, D.M., Heinz, D.L., Prakapenka, V., 2013. High-pressure high-temperature equations of state of UO_2 and ThO_2. AGU Fall Meet. Abstr. A2319.

Chollet, M., Belin, R., Richaud, J., 2013. High-temperature X-ray diffraction study of uranium–neptunium mixed oxides. Inorg. Chem. 52, 2519–2525. http://dx.doi.org/10.1021/ic302457m.

Chute, J.H., 1967. Direct observation of fission fragment damage in some ceramic oxides. J. Nucl. Mater 21, 77–87. http://dx.doi.org/10.1016/0022-3115(67)90731-3.

Clavier, N., Podor, R., Deliere, L., Ravaux, J., Dacheux, N., 2013. Combining in situ HT-ESEM observations and dilatometry: an original and fast way to the sintering map of ThO_2. Mater. Chem. Phys. 137, 742–749. http://dx.doi.org/10.1016/j.matchemphys.2012.10.003.

Conradson, S.D., Abney, K.D., Begg, B.D., Brady, E.D., Clark, D.L., den Auwer, C., Ding, M., Dorhout, P.K., Espinosa-Faller, F.J., Gordon, P.L., Haire, R.G., Hess, N.J., Hess, R.F., Keogh, D.W., Lander, G.H., Lupinetti, A.J., Morales, L.A., Neu, M.P., Palmer, P.D., Paviet-Hartmann, P., Reilly, S.D., Runde, W.H., Tait, C.D., Veirs, D.K., Wastin, F., 2004a. Higher order speciation effects on plutonium L_3 X-ray absorption near edge spectra. Inorg. Chem. 43, 116–131. http://dx.doi.org/10.1021/ic0346477.

Conradson, S.D., Manara, D., Wastin, F., Clark, D.L., Lander, G.H., Morales, L.A., Rebizant, J., Rondinella, V.V., 2004b. Local structure and charge distribution in the UO_2-U_4O_9 system. Inorg. Chem. 43, 6922–6935. http://dx.doi.org/10.1021/ic049748z.

Degueldre, C., 2007. Zirconia inert matrix for plutonium utilisation and minor actinides disposition in reactors. J. Alloys Comp. 444–445, 36–41. http://dx.doi.org/10.1016/j.jallcom.2006.11.203.

Degueldre, C., Paratte, J., 1999. Concepts for an inert matrix fuel, an overview. J. Nucl. Mater 274, 1–6. http://dx.doi.org/10.1016/S0022-3115(99)00060-4.

Desgranges, L., Baldinozzi, G., Ruello, P., Petot, C., 2012. Is UO_2 irradiation resistance due to its unusual high temperature behaviour? J. Nucl. Mater 420, 334–337. http://dx.doi.org/10.1016/j.jnucmat.2011.10.003.

Douglass, D., Bronisz, S., 1971. Alpha particle irradiation damage in ThO_2. J. Am. Ceram. Soc. 54, 158–161. http://dx.doi.org/10.1111/j.1151-2916.1971.tb12245.x.

Duffy, D.M., Daraszewicz, S.L., Mulroue, J., 2012. Modelling the effects of electronic excitations in ionic-covalent materials. Nucl. Instrum. Meth. B 277, 21–27. http://dx.doi.org/10.1016/j.nimb.2011.12.059.

Errandonea, D., Kumar, R., Gracia, L., Beltrán, A., Achary, S., Tyagi, A., 2009. Experimental and theoretical investigation of $ThGeO_4$ at high pressure. Phys. Rev. B 80, 094101. http://dx.doi.org/10.1103/PhysRevB.80.094101.

Ewing, R.C., 2007. Ceramic matrices for plutonium disposition. Prog. Nucl. Energy 49, 635–643. http://dx.doi.org/10.1016/j.pnucene.2007.02.003.

Ewing, R.C., 2011. Safe management of actinides in the nuclear fuel cycle: role of mineralogy. Comptes Rendus Geosci. 343, 219–229. http://dx.doi.org/10.1016/j.crte.2010.09.003.

Ewing, R.C., Meldrum, A., Wang, L., Wang, S., 2000. Radiation-induced amorphization. Rev. Mineral. Geochem. 39, 319–361. http://dx.doi.org/10.2138/rmg.2000.39.12.

Ewing, R.C., Weber, W.J., Lian, J., 2004. Nuclear waste disposal—pyrochlore ($A_2B_2O_7$): nuclear waste form for the immobilization of plutonium and "minor" actinides. J. Appl. Phys. 95, 5949. http://dx.doi.org/10.1063/1.1707213.

Eyal, Y., Abu Saleh, S., 2007. Structure model and small-angle scattering cross sections of latent ion tracks in dielectric solids. J. Appl. Crystallogr. 40, 71–76. http://dx.doi.org/10.1107/S0021889806042634.

Finch, R., Murakami, T., 1999. Systematics and paragenesis of uranium minerals. Rev. Mineral. 38, 91–179.

Fleischer, R.L., 2004. Fission tracks in solids — production mechanisms and natural origins. J. Mater. Sci. 39, 3901–3911. http://dx.doi.org/10.1023/B:JMSC.0000031471.17343.32.

Garrido, F., Choffel, C., Dran, J., Thorn, L., Nowicki, L., Turos, A., 1997. Structural modifications in uranium dioxide irradiated with swift heavy ions. Nucl. Instrum. Meth. B 128, 634–638. http://dx.doi.org/10.1016/S0168-583X(96)01142-1.

Garrido, F., Moll, S., Sattonnay, G., Thomé, L., Vincent, L., 2009. Radiation tolerance of fluorite-structured oxides subjected to swift heavy ion irradiation. Nucl. Instrum. Meth. B 267, 1451–1455. http://dx.doi.org/10.1016/j.nimb.2009.01.070.

Greaux, S., Gautron, L., Andrault, D., Bolfan-Casanova, N., Guignot, N., Haines, J., 2008. Structural characterization of natural UO_2 at pressures up to 82 GPa and

temperatures up to 2200 K. Am. Mineral. 93, 1090–1098. http://dx.doi.org/10.2138/am.2008.2735.
Grimes, R.W., Konings, R.J.M., Edwards, L., 2008. Greater tolerance for nuclear materials. Nat. Mater 7, 683–685. http://dx.doi.org/10.1038/nmat2266.
Guimbretière, G., Desgranges, L., Canizarès, A., Carlot, G., Caraballo, R., Jégou, C., Duval, F., Raimboux, N., Ammar, M.R., Simon, P., 2012. Determination of in-depth damaged profile by Raman line scan in a pre-cut He^{2+} irradiated UO_2. Appl. Phys. Lett. 100, 251914. http://dx.doi.org/10.1063/1.4729588.
Hayashi, K., Kikuchi, H., Fukuda, K., 1994. Radiation damage of UO_2 implanted with 100 MeV iodine ions. J. Alloys Comp. 213–214, 351–353. http://dx.doi.org/10.1016/0925-8388(94)90929-6.
Hayashi, K., Kikuchi, H., Fukuda, K., 1997. Radiation damage of UO_2 by high-energy heavy ions. J. Nucl. Mater 248, 191–195. http://dx.doi.org/10.1016/S0022-3115(97)00119-0.
Helffrich, G., Wood, B., 2001. The Earth's mantle. Nature 412, 501–507. http://dx.doi.org/10.1038/35087500.
Hobbs, L.W., Clinard, F.W., Zinkle, S.J., Ewing, R.C., Ridge, O., 1994. Radiation effects in ceramics. J. Nucl. Mater 216, 291–321. http://dx.doi.org/10.1016/0022-3115(94)90017-5.
Horlait, D., Caraballo, R., Lebreton, F., Jégou, C., Roussel, P., Delahaye, T., 2014. Self-irradiation and oxidation effects on americium sesquioxide and Raman spectroscopy studies of americium oxides. J. Solid State Chem. 217, 159–168. http://dx.doi.org/10.1016/j.jssc.2014.05.025.
Hurtgen, C., Fuger, J., 1977. Self-irradiation effects in americium oxides. Inorg. Nucl. Chem. Lett. 13, 179–188. http://dx.doi.org/10.1016/0020-1650(77)80091-3.
Idiri, M., Le Bihan, T., Heathman, S., Rebizant, J., 2004. Behavior of actinide dioxides under pressure: UO_2 and ThO_2. Phys. Rev. B 70, 014113. http://dx.doi.org/10.1103/PhysRevB.70.014113.
Ishikawa, N., Sonoda, T., Sawabe, T., Sugai, H., Sataka, M., 2013. Electronic stopping power dependence of ion-track size in UO2 irradiated with heavy ions in the energy range of ~1 MeV/u. Nucl. Instrum. Meth. B 314, 180–184. http://dx.doi.org/10.1016/j.nimb.2013.05.038.
Jayaraman, A., 1986. Ultrahigh pressures. Rev. Sci. Instrum. 57, 1013. http://dx.doi.org/10.1063/1.1138654.
Jayaraman, A., Kourouklis, G., Uitert Van, L., 1988. A high pressure raman study of ThO_2 to 40 GPa and pressure-induced phase transition from fluorite structure. Pramana 30, 225–231. http://dx.doi.org/10.1007/BF02846696.
Knittle, E., 1993. High-pressure Raman spectroscopy of $ZrSiO_4$: observation of the zircon to scheelite transition at 300 K. Am. Min. 78, 245–252.
Krupa, J.C., 2005. High-energy optical absorption in f −compounds. J. Solis State Chem. 178, 483–488. http://dx.doi.org/10.1016/j.jssc.2004.11.033.
Lang, M., Glasmacher, U.A., Neumann, R., Schardt, D., Trautmann, C., Wagner, G.A., 2005. Energy loss of 50-GeV uranium ions in natural diamond. Appl. Phys. A 80, 691–694. http://dx.doi.org/10.1007/s00339-004-3104-1.
Lang, M., Lian, J., Zhang, F., Hendriks, B.W.H., Trautmann, C., Neumann, R., Ewing, R.C., 2008. Fission tracks simulated by swift heavy ions at crustal pressures and temperatures. Earth Planet. Sci. Lett. 274, 355–358. http://dx.doi.org/10.1016/j.epsl.2008.07.039.
Lang, M., Lian, J., Zhang, J., Zhang, F., Weber, W.J., Trautmann, C., Ewing, R.C., 2009a. Single-ion tracks in $Gd_2Zr_{2-x}Ti_xO_7$ pyrochlores irradiated with swift heavy ions. Phys. Rev. B 79, 224105. http://dx.doi.org/10.1103/PhysRevB.79.224105.
Lang, M., Toulemonde, M., Zhang, J., Zhang, F., Tracy, C.L., Lian, J., Wang, Z., Weber, W.J., Severin, D., Bender, M., Trautmann, C., Ewing, R.C., 2014. Swift heavy ion track formation in $Gd_2Zr_{2-x}Ti_xO_7$ pyrochlore: effect of electronic energy loss. Nucl. Instrum. Meth. B 336, 102–115. http://dx.doi.org/10.1016/j.nimb.2014.06.019.
Lang, M., Tracy, C.L., Palomares, R.I., Zhang, F., Severin, D., Bender, M., Trautmann, C., Park, C., Prakapenka, V.B., Skuratov, V.A., Ewing, R.C., 2015. Characterization of ion-induced radiation effects in nuclear materials using synchrotron x-ray techniques. J. Mater. Res. 30, 1366–1379. http://dx.doi.org/10.1557/jmr.2015.6.
Lang, M., Zhang, F., Ewing, R.C., Lian, J., Trautmann, C., Wang, Z., 2009b. Structural modifications of $Gd_2Zr_{2-x}Ti_xO_7$ pyrochlore induced by swift heavy ions: disordering and amorphization. J. Mater. Res. 24, 1322–1334. http://dx.doi.org/10.1557/jmr.2009.0151.
Lang, M., Zhang, F., Li, W., Severin, D., 2012. Swift heavy ion-induced amorphization of $CaZrO_3$ perovskite. Nucl. Instrum. Meth. B 286, 271–276. http://dx.doi.org/10.1016/j.nimb.2011.12.028.
Lang, M., Zhang, F., Lian, J., Trautmann, C., Neumann, R., Ewing, R.C., 2009c. Combined high pressure and heavy-ion irradiation: a novel approach. J. Synchrotron Radiat. 16, 773–777. http://dx.doi.org/10.1107/S0909049509034384.
Lang, M., Zhang, F., Zhang, J., Wang, J., Lian, J., Weber, W.J., Schuster, B., Trautmann, C., Neumann, R., Ewing, R.C., 2010. Review of $A_2B_2O_7$ pyrochlore response to irradiation and pressure. Nucl. Instrum. Meth. B 268, 2951–2959. http://dx.doi.org/10.1016/j.nimb.2010.05.016.
Lang, M., Zhang, F., Zhang, J., Wang, J., Schuster, B., Trautmann, C., Neumann, R., Becker, U., Ewing, R.C., 2009d. Nanoscale manipulation of the properties of solids at high pressure with relativistic heavy ions. Nat. Mater 8, 793–797. http://dx.doi.org/10.1038/nmat2528.
Laverov, N.P., Yudintsev, S.V., Velichkin, V.I., Lukinykh, A.N., Tomilin, S.V., Lizin, A.A., Stefanovskii, S.V., 2009. Effect of amorphization on isolation properties of actinide pyrochlore matrix. Radiochemistry 51, 529–536. http://dx.doi.org/10.1134/S1066362209050178.
Lebreton, F., Belin, R.C., Prieur, D., Delahaye, T., Blanchart, P., 2012. In situ study of the solid-state formation of $U_{1-x}Am_xO_{2\pm\delta}$ solid solution. Inorg. Chem. 51, 9369–9375. http://dx.doi.org/10.1021/ic301124d.
Li, W., Wang, L., Lang, M., Trautmann, C., Ewing, R.C., 2011. Thermal annealing mechanisms of latent fission tracks: apatite vs. zircon. Earth Planet. Sci. Lett. 302, 227–235. http://dx.doi.org/10.1016/j.epsl.2010.12.016.
Liu, J., Glasmacher, U.A., Lang, M., Trautmann, C., Voss, K.-O., Neumann, R., Wagner, G.A., Miletich, R., 2008. Raman spectroscopy of apatite irradiated with swift heavy ions with and without simultaneous exertion of high pressure. Appl. Phys. A 91, 17–22. http://dx.doi.org/10.1007/s00339-008-4402-9.
Liu, L.-G., 1980. High-pressure phase transformations of fluorite-type dioxides. Earth Planet. Sci. Lett. 49, 166–172. http://dx.doi.org/10.1016/0012-821X(80)90158-2.
Liu, L.-G., 1979. High-pressure phase transformations in baddeleyite and zircon, with geophysical implications. Earth Planet. Sci. Lett. 44, 390–396. http://dx.doi.org/10.1016/0012-821X(79)90078-5.
Livshits, T.S., Lizin, A.A., Zhang, J., Ewing, R.C., 2010. Amorphization of rare earth aluminate garnets under ion irradiation and decay of ^{244}Cm admixture. Geol. Ore Depos. 52, 267–278. http://dx.doi.org/10.1134/S1075701510040021.
Lombardi, C., Luzzi, L., Padovani, E., Vettraino, F., 2008. Thoria and inert matrix fuels for a sustainable nuclear power. Prog. Nucl. Energy 50, 944–953. http://dx.doi.org/10.1016/j.pnucene.2008.03.006.
Lumpkin, G.R., 2001. Alpha-decay damage and aqueous durability of actinide host phases in natural systems. J. Nucl. Mater 289, 136–166. http://dx.doi.org/10.1016/S0022-3115(00)00693-0.
Lung, M., Gremm, O., 2000. Perspectives of the thorium fuel cycle. Nucl. Eng. Des. 180, 133–146. http://dx.doi.org/10.1016/S0029-5493(97)00296-3.
Manara, D., Pflieger, R., Sheindlin, M., 2005a. Advances in the experimental determination of the uranium–oxygen phase diagram at high temperature. Int. J. Thermophys. 26, 1193–1206. http://dx.doi.org/10.1007/s10765-005-6711-y.
Manara, D., Ronchi, C., Sheindlin, M., 2002. Pressure dependence of UO_2 melting measured by double-pulse laser heating. Int. J. Thermophys. 23, 1147–1156. http://dx.doi.org/10.1023/A:1019879917797.
Manara, D., Ronchi, C., Sheindlin, M., Lewis, M., Brykin, M., 2005b. Melting of stoichiometric and hyperstoichiometric uranium dioxide. J. Nucl. Mater 342, 148–163. http://dx.doi.org/10.1016/j.jnucmat.2005.04.002.
Manara, D., Sheindlin, M., Lewis, M., 2004. Advances in measurements of the melting transition in non-stoichiometric UO_2. Int. J. Thermophys. 25, 533–545. http://dx.doi.org/10.1023/B: IJOT.0000028488.43690.7d.
Martin, P.M., Belin, R.C., Valenza, P.J., Scheinost, A.C., 2009. EXAFS study of the structural phase transition in the americium zirconate pyrochlore. J. Nucl. Mater 385, 126–130. http://dx.doi.org/10.1016/j.jnucmat.2008.10.028.
Matzke, H., 1992. Radiation damage in nuclear materials. Nucl. Instrum. Meth. B 65, 30–39. http://dx.doi.org/10.1016/0168-583X(92)95010-O.
Mieszczynski, C., Degueldre, C., Kuri, G., Bertsch, J., Borca, C.N., 2012. Investigation of irradiated uranium-plutonium mixed oxide fuel by synchrotron based micro X-ray diffraction. Prog. Nucl. Energy 57, 130–137. http://dx.doi.org/10.1016/j.pnucene.2011.11.012.
Mieszczynski, C., Kuri, G., Degueldre, C., Martin, M., Bertsch, J., Borca, C.N., Grolimund, D., Delafoy, C., Simoni, E., 2014. Irradiation effects and microstructural changes in large grain uranium dioxide fuel investigated by microbeam X-ray diffraction. J. Nucl. Mater 444, 274–282. http://dx.doi.org/10.1016/j.jnucmat.2013.09.054.
Miro, S., Costantini, J.M., Bardeau, J.F., Chateigner, D., Studer, F., Balanzat, E., 2011. Raman spectroscopy study of damage induced in fluorapatite by swift heavy ion irradiations. J. Raman Spectrosc. 2011, 2036–2041. http://dx.doi.org/10.1002/jrs.2955.
Miro, S., Grebille, D., Chateigner, D., Pelloquin, D., Stoquert, J., Grob, J., Costantini, J., Studer, F., 2005. X-ray diffraction study of damage induced by swift heavy ion irradiation in fluorapatite. Nucl. Instrum. Meth. B 227, 306–318. http://dx.doi.org/10.1016/j.nimb.2004.08.025.
Molodets, A.M., Fortov, V.E., 2004. Phase transitions in uranium dioxide at high pressures and temperatures. J. Exp. Theor. Phys. Lett. 80, 172–175. http://dx.doi.org/10.1134/1.1808844.
Nakae, N., Harada, A., Kirihara, T., Nasu, S., 1978a. Irradiation induced lattice defects in UO_2. J. Nucl. Mater 71, 314–319. http://dx.doi.org/10.1016/0022-3115(78)90430-0.
Nakae, N., Iwata, Y., Kirihara, T., 1979. Thermal recovery of defects in neutron irradiated UO_2. J. Nucl. Mater 80, 314–322. http://dx.doi.org/10.1016/0022-3115(79)90194-6.
Nakae, N., Kirihara, T., Nasu, S., 1978b. Irradiation induced volume change in UO_2. J. Nucl. Mater 74, 1–9. http://dx.doi.org/10.1016/0022-3115(78)90526-3.
Nishi, T., Nakada, M., Suzuki, C., Shibata, H., Itoh, A., Akabori, M., Hirata, M., 2010. Local and electronic structure of Am_2O_3 and AmO_2 with XAFS spectroscopy. J. Nucl. Mater 401, 138–142. http://dx.doi.org/10.1016/j.jnucmat.2010.04.011.
Noggle, T.S., Stiegler, J.O., 1960. Electron microscope observations of fission fragment tracks in thin films of UO_2. J. Appl. Phys. 31, 2199–2208. http://dx.doi.org/10.1063/1.1735523.
Nogita, K., Une, K., 1994. Radiation-induced microstructural change in high burnup UO_2 fuel pellets. Nucl. Instrum. Meth. B 91, 301–306. http://dx.doi.org/10.1016/0168-583X(94)96235-9.
Otobe, H., Takano, M., Hayashi, H., Arai, Y., 2011. Oxygen potentials of pyrochlore-type $Am_2Zr_2O_{7+y}$. J. Am. Ceram. Soc. 94, 3596–3599. http://dx.doi.org/10.1111/j.1551-2916.2011.04617.x.
Palomares, R.I., Tracy, C.L., Zhang, F., Park, C., Popov, D., Trautmann, C., Ewing, R.C., Lang, M., 2015. In situ defect annealing of swift heavy ion irradiated CeO_2 and ThO_2 using synchrotron X-ray diffraction and a hydrothermal diamond anvil cell. J. Appl. Cryst. 48, 711–717. http://dx.doi.org/10.1107/S160057671500477X.

Park, S., Lang, M., Tracy, C.L., Zhang, J., Zhang, F., Trautmann, C., Rodriguez, M.D., Kluth, P., Ewing, R.C., 2015. Response of $Gd_2Ti_2O_7$ and $La_2Ti_2O_7$ to swift-heavy ion irradiation and annealing. Acta. Mater 93, 1–11. http://dx.doi.org/10.1016/j.actamat.2015.04.010.

Patel, M.K., Avasthi, D.K., Kulriya, P.K., Kailas, S., Pivin, J.C., Tyagi, A.K., Vijayakumar, V., 2010. Swift heavy ion induced structural modifications in zircon and scheelite phases of $ThGeO_4$. Nucl. Instrum. Meth. B 268, 42–48. http://dx.doi.org/10.1016/j.nimb.2009.09.026.

Prieur, D., Martin, P.M., Lebreton, F., Delahaye, T., Jankowiak, A., Laval, J.-P., Scheinost, A.C., Dehaudt, P., Blanchart, P., 2012. Alpha self-irradiation effect on the local structure of the $U_{0.85}Am_{0.15}O_{2\pm x}$ solid solution. J. Solid State Chem. 194, 206–211. http://dx.doi.org/10.1016/j.jssc.2012.05.006.

Prieur, D., Vigier, J.-F., Wiss, T., Janssen, A., Rothe, J., Cambriani, A., Somers, J., 2014. Structural investigation of self-irradiation damaged AmO_2. J. Solid State Chem. 212, 7–12. http://dx.doi.org/10.1016/j.jssc.2013.12.016.

Rietveld, H.M., 1969. A profile refinement method for nuclear and magnetic structures. J. Appl. Crystallogr. 2, 65–71. http://dx.doi.org/10.1107/S0021889869006558.

Robinson, M., 1994. Basic physics of radiation damage production. J. Nucl. Mater 216, 1–28. http://dx.doi.org/10.1016/0022-3115(94)90003-5.

Ronchi, C., 1973. The nature of surface fission tracks in UO_2. J. Appl. Phys. 44, 3575–3585. http://dx.doi.org/10.1063/1.1662802.

Ronchi, C., Wiss, T., 2002. Fission-fragment spikes in uranium dioxide. J. Appl. Phys. 92, 5837. http://dx.doi.org/10.1063/1.1513192.

Ruello, P., Desgranges, L., Baldinozzi, G., Calvarin, G., Hansen, T., Petot-Ervas, G., Petot, C., 2005. Heat capacity anomaly in UO_2 in the vicinity of 1300 K: an improved description based on high resolution X-ray and neutron powder diffraction studies. J. Phys. Chem. Solids 66, 823–831. http://dx.doi.org/10.1016/j.jpcs.2004.10.009.

Sapelkin, A., Bayliss, S., 2001. X-ray absorption spectroscopy under high pressures in diamond anvil cells. Int. J. High. Press. Res. 21, 315–329. http://dx.doi.org/10.1080/08957950108202590.

Sattonnay, G., Moll, S., Thomé, L., Decorse, C., Legros, C., Simon, P., Jagielski, J., Jozwik, I., Monnet, I., 2010. Phase transformations induced by high electronic excitation in ion-irradiated $Gd_2(Zr_xTi_{1-x})_2O_7$ pyrochlores. J. Appl. Phys. 108, 103512. http://dx.doi.org/10.1063/1.3503452.

Sattonnay, G., Moll, S., Thomé, L., Legros, C., Calvo, A., Herbst-Ghysel, M., Decorse, C., Monnet, I., 2012. Effect of composition on the behavior of pyrochlores irradiated with swift heavy ions. Nucl. Instrum. Meth. B 272, 261–265. http://dx.doi.org/10.1016/j.nimb.2011.01.079.

Schuster, B., Fujara, F., Merk, B., Neumann, R., Seidl, T., Trautmann, C., 2012. Response behavior of ZrO_2 under swift heavy ion irradiation with and without external pressure. Nucl. Instrum. Meth. B 277, 45–52. http://dx.doi.org/10.1016/j.nimb.2011.12.060.

Schuster, B., Lang, M., Klein, R., Trautmann, C., Neumann, R., Benyagoub, A., 2009. Structural phase transition in ZrO_2 induced by swift heavy ion irradiation at high-pressure. Nucl. Instrum. Meth. B 267, 964–968. http://dx.doi.org/10.1016/j.nimb.2009.02.046.

Shi, W.-Q., Yuan, L.-Y., Wang, C.-Z., Wang, L., Mei, L., Xiao, C.-L., Zhang, L., Li, Z.-J., Zhao, Y.-L., Chai, Z.-F., 2014. Exploring actinide materials through synchrotron radiation techniques. Adv. Mater 1–42. http://dx.doi.org/10.1002/adma.201304323.

Sickafus, K.E., Grimes, R.W., Valdez, J.A., Cleave, A., Tang, M., Ishimaru, M., Corish, S.M., Stanek, C.R., Uberuaga, B.P., 2007. Radiation-induced amorphization resistance and radiation tolerance in structurally related oxides. Nat. Mater 6, 217–223. http://dx.doi.org/10.1038/nmat1842.

Sickafus, K.E., Minervini, L., Grimes, R., Valdez, J., Ishimaru, M., Li, F., McClellan, K., Hartmann, T., 2000. Radiation tolerance of complex oxides. Science 289, 748–751. http://dx.doi.org/10.1126/science.289.5480.748.

Skinner, L.B., Benmore, C.J., Weber, J.K.R., Williamson, M.A., Tamalonis, A., Hebden, A., Wiencek, T., Alderman, O.L.G., Guthrie, M., Leibowitz, L., Parise, J.B., 2014. Molten uranium dioxide structure and dynamics. Science 346, 984–987. http://dx.doi.org/10.1126/science.1259709.

Sonoda, T., Kinoshita, M., Chimi, Y., Ishikawa, N., Sataka, M., Iwase, A., 2006. Electronic excitation effects in CeO_2 under irradiations with high-energy ions of typical fission products. Nucl. Instrum. Meth. B 250, 254–258. http://dx.doi.org/10.1016/j.nimb.2006.04.120.

Sonoda, T., Kinoshita, M., Ishikawa, N., Sataka, M., Iwase, A., Yasunaga, K., 2010. Clarification of high density electronic excitation effects on the microstructural evolution in UO_2. Nucl. Instrum. Meth. B 268, 3277–3281. http://dx.doi.org/10.1016/j.nimb.2010.06.015.

Subramanian, M., Aravamudan, G., Subba Rao, G., 1983. Oxide pyrochlores–A review. Prog. Solid State Chem. 15, 55–143. http://dx.doi.org/10.1016/0079-6786(83)90001-8.

Sureda, R., Casas, I., Gim, J., de Pablo, J., Quinones, J., Zhang, J., Ewing, R.C., 2011. Effects of ionizing radiation and temperature on uranyl silicates: soddyite $(UO_2)_2(SiO_4)(H_2O)_2$ and uranophane $Ca(UO_2)_2(SiO_3OH)_25H_2O$. Environ. Sci. Technol. 2, 2510–2515. http://dx.doi.org/10.1021/es1041496.

Sykora, R.E., Raison, P.E., Haire, R.G., 2005. Self-irradiation induced structural changes in the transplutonium pyrochlores $An_2Zr_2O_7$ (An=Am, Cf). J. Solid State Chem. 178, 578–583. http://dx.doi.org/10.1016/j.jssc.2004.07.037.

Takaki, S., Yasuda, K., Yamamoto, T., Matsumura, S., Ishikawa, N., 2014. Atomic structure of ion tracks in Ceria. Nucl. Instrum. Meth. B 326, 140–144. http://dx.doi.org/10.1016/j.nimb.2013.10.077.

Thomé, L., Debelle, A., Garrido, F., Mylonas, S., Décamps, B., Bachelet, C., Sattonnay, G., Moll, S., Pellegrino, S., Miro, S., Trocellier, P., Serruys, Y., Velisa, G., Grygiel, C., Monnet, I., Toulemonde, M., Simon, P., Jagielski, J., Jozwik-Biala, I., Nowicki, L., Behar, M., Weber, W.J., Zhang, Y., Backman, M., Nordlund, K., Djurabekova, F., 2013. Radiation effects in nuclear materials: role of nuclear and electronic energy losses and their synergy. Nucl. Instrum. Meth. B. http://dx.doi.org/10.1016/j.nimb.2012.11.077.

Trachenko, K., Brazhkin, V., Tsiok, O., Dove, M., Salje, E., 2007. Pressure-induced structural transformation in radiation-amorphized zircon. Phys. Rev. Lett. 98, 135502. http://dx.doi.org/10.1103/PhysRevLett.98.135502.

Tracy, C.L., Lang, M., Pray, J.M., Zhang, F., Popov, D., Park, C., Trautmann, C., Bender, M., Severin, D., Skuratov, V.A., Ewing, R.C., 2015a. Redox response of actinide materials to highly-ionizing radiation. Nat. Commun. 6, 6133. http://dx.doi.org/10.1038/ncomms7133.

Tracy, C.L., Lang, M., Zhang, F., Trautmann, C., Ewing, R.C., 2015b. Phase transformations in Ln_2O_3 materials irradiated with swift heavy ions. Phys. Rev. B 92, 174101. http://dx.doi.org/10.1103/PhysRevB.92.174101.

Tracy, C.L., Lang, M., Zhang, J., Zhang, F., 2012. Structural response of A_2TiO_5 (A= La, Nd, Sm, Gd) to swift heavy ion irradiation. Acta Mater 60, 4477–4486. http://dx.doi.org/10.1016/j.actamat.2012.05.005.

Tracy, C.L., McLain Pray, J., Lang, M., Popov, D., Park, C., Trautmann, C., Ewing, R.C., 2014. Defect accumulation in ThO_2 irradiated with swift heavy ions. Nucl. Instrum. Meth. B 326, 169–173. http://dx.doi.org/10.1016/j.nimb.2013.08.070.

Tschauner, O., Ma, C., Grubor-Urosevic, O., Chen, Y.J., 2013. Anomalous bulk compression behaviour in a hyperstoichiometric uranium-dioxide-thorium-dioxide solid solution. J. Phys. Condens. Matter 25, 162201. http://dx.doi.org/10.1088/0953-8984/25/16/162201.

Turcotte, D.L., Paul, D., White, W.M., 2001. Thorium-uranium systematics require layered mantle convection. J. Geophys. Res. 106, 4265–4276. http://dx.doi.org/10.1029/2000JB900409.

Utsunomiya, S., Wang, L., Douglass, M., Clark, S., Ewing, R., 2003. The effect of ionizing radiation on uranophane. Am. Mineral. 88, 159–166. http://dx.doi.org/10.1021/es1041496.

Vauchy, R., Belin, R.C., Robisson, A.-C., Hodaj, F., 2014. High temperature X-ray diffraction study of the kinetics of phase separation in hypostoichiometric uranium–plutonium mixed oxides. J. Eur. Ceram. Soc. 34, 2543–2551. http://dx.doi.org/10.1016/j.jeurceramsoc.2014.02.028.

Wallmann, J.C., 1964. A structural transformation of curium sesquioxide. J. Inorg. Nucl. Chem. 26, 2053–2057. http://dx.doi.org/10.1016/0022-1902(64)80149-4.

Weber, W., Ewing, R., 1998. Radiation effects in crystalline ceramics for the immobilization of high-level nuclear waste and plutonium. J. Mater. Res. 13, 1434–1484. http://dx.doi.org/10.1557/JMR.1998.0205.

Weber, W.J., 1981. Ingrowth of lattice defects in alpha irradiated UO_2 single crystals. J. Nucl. Mater 98, 206–215. http://dx.doi.org/10.1016/0022-3115(81)90400-1.

Weber, W.J., 1983. Thermal recovery of lattice defects in alpha-irradiated UO_2 crystals. J. Nucl. Mater 114, 213–221. http://dx.doi.org/10.1016/0022-3115(83)90259-3.

Weber, W.J., 1984. Alpha-irradiation damage in CeO_2, UO_2 and PuO_2. Radiat. Eff. 83, 145–156. http://dx.doi.org/10.1080/00337578408215798.

Weber, W.J., 2000. Models and mechanisms of irradiation-induced amorphization in ceramics. Nucl. Instrum. Meth. B 166–167, 98–106. http://dx.doi.org/10.1016/S0168-583X(99)00643-6.

Weikusat, C., Glasmacher, U.A., Schuster, B., Trautmann, C., Miletich, R., Neumann, R., 2010. Raman study of apatite amorphised with swift heavy ions under various irradiation conditions. Phys. Chem. Min. 38, 293–303. http://dx.doi.org/10.1007/s00269-010-0403-2.

West, R.G., Blankenship, A.C., Vassiliev, A., Gorter, W., Anderson, C., Schieber, M., Pointon, A.J., Robertson, J.M., Ferrite, N., Sucksmith, W., Feitknecht, W., Mannweiler, U., Strickler, P.W., Roy, R., 1968. Annealing of irradiation-induced thermal conductivity changes in ThO_2-1.3 wt% UO_2. J. Am. Ceram. Soc. 52, 160–165. http://dx.doi.org/10.1111/j.1151-2916.1969.tb11205.x.

Williamson, G., Hall, W., 1953. X-ray line broadening from filed aluminium and wolfram. Acta Metall. 1, 22–31. http://dx.doi.org/10.1016/0001-6160(53)90006-6.

Wiss, T., 1999. Heavy ion induced damage in $MgAl_2O_4$, an inert matrix candidate for the transmutation of minor actinides. Radiat. Meas. 31, 507–514. http://dx.doi.org/10.1016/S1350-4487(99)00113-4.

Wiss, T., Hiernaut, J.-P., Roudil, D., Colle, J.-Y., Maugeri, E., Talip, Z., Janssen, A., Rondinella, V., Konings, R.J.M., Matzke, H.-J., Weber, W.J., 2014. Evolution of spent nuclear fuel in dry storage conditions for millennia and beyond. J. Nucl. Mater 451, 198–206. http://dx.doi.org/10.1016/j.jnucmat.2014.03.055.

Wiss, T., Matzke, H., 1997. Radiation damage in UO_2 by swift heavy ions. Nucl. Instrum. Meth. B 122, 583–588. http://dx.doi.org/10.1016/S0168-583X(96)00754-9.

Wuensch, B., Eberman, K., Heremans, C., 2000. Connection between oxygen-ion conductivity of pyrochlore fuel-cell materials and structural change with composition and temperature. Solid State Ionics 129, 111–133. http://dx.doi.org/10.1016/S0167-2738(99)00320-3.

Xiao, H.Y., Zhang, F., Gao, F., Lang, M., Ewing, R.C., Weber, W.J., 2010. Zirconate pyrochlores under high pressure. Phys. Chem. Chem. Phys. 12, 12472–12477. http://dx.doi.org/10.1039/c0cp00278j.

Zhang, F., Lang, M., Liu, Z., Ewing, R.C., 2011a. Phase stability of some actinides with brannerite structure at high pressures. J. Solid State Chem. 184, 2834–2839. http://dx.doi.org/10.1016/j.jssc.2011.08.022.

Zhang, F., Lang, M., Tracy, C., Ewing, R.C., Gregg, D.J., Lumpkin, G.R., 2014a. Incorporation of uranium in pyrochlore oxides and pressure-induced phase

transitions. J. Solid State Chem. 219, 49–54. http://dx.doi.org/10.1016/j.jssc.2014.07.011.

Zhang, F., Lang, M., Wang, J.W., Li, W.X., Sun, K., Prakapenka, V., Ewing, R.C., 2014b. High-pressure U3O8 with the fluorite-type structure. J. Solid State Chem. 213, 110–115. http://dx.doi.org/10.1016/j.jssc.2014.02.012.

Zhang, F., Pointeau, V., Shuller, L.C., Reaman, D.M., Lang, M., Liu, Z., Hu, J., Panero, W.R., Becker, U., Poinssot, C., Ewing, R.C., 2009. Structural transitions and electron transfer in coffinite, USiO4, at high pressure. Am. Mineral. 94, 916–920. http://dx.doi.org/10.2138/am.2009.3111.

Zhang, F., Wang, J., Lian, J., Lang, M., Becker, U., Ewing, R.C., 2008. Phase stability and pressure dependence of defect formation in $Gd_2Ti_2O_7$ and $Gd_2Zr_2O_7$ pyrochlores. Phys. Rev. Lett. 100, 045503. http://dx.doi.org/10.1103/PhysRevLett.100.045503.

Zhang, J., Lang, M., Ewing, R.C., Devanathan, R., Weber, W.J., Toulemonde, M., 2011b. Nanoscale phase transitions under extreme conditions within an ion track. J. Mater. Res. 25, 1344–1351. http://dx.doi.org/10.1557/JMR.2010.0180.